

The potential of X-ray cluster surveys to constrain primordial non-Gaussianity

B. Sartoris^{1,2,3}, S. Borgani^{1,2,3}, C. Fedeli^{4,5,6}, S. Matarrese^{7,8}, L. Moscardini^{4,5,6},
 P. Rosati⁹ and J. Weller^{10,11}

¹ Dipartimento di Fisica, Sezione di Astronomia, Università di Trieste, Via Tiepolo 11, I-34143 Trieste, Italy

² INAF-Osservatorio Astronomico di Trieste, Via Tiepolo 11, I-34143 Trieste, Italy

³ INFN, Sezione di Trieste, Via Valerio 2, I-34127 Trieste, Italy

⁴ Dipartimento di Astronomia, Università di Bologna, Via Ranzani 1, I-40127 Bologna, Italy

⁵ INAF-Osservatorio Astronomico di Bologna, Via Ranzani 1, I-40127 Bologna, Italy

⁶ INFN, Sezione di Bologna, Viale Berti Pichat 6/2, I-40127 Bologna, Italy

⁷ Dipartimento di Fisica “G. Galilei”, Università di Padova, via Marzolo 8, I-35131, Padova, Italy

⁸ INFN – Sezione di Padova, via Marzolo 8, I-35131, Padova, Italy

⁹ ESO-European Southern Observatory, D-85748 Garching bei München, Germany

¹⁰ University Observatory, Ludwig-Maximilians University Munich, Scheinerstr. 1, 81679 Munich, Germany

¹¹ Excellence Cluster Universe, Boltzmannstr. 2, 85748 Garching, Germany

23 March 2022

ABSTRACT

We present forecasts for constraints on deviations from Gaussian distribution of primordial density perturbations from future high-sensitivity X-ray surveys of galaxy clusters. Our analysis is based on computing the Fisher-Matrix for number counts and large-scale power spectrum of clusters. The surveys that we consider have high-sensitivity and wide-area to detect about 2.5×10^5 extended sources, and to provide reliable measurements of robust mass proxies for about 2×10^4 clusters. Based on the so-called self-calibration approach, and including Planck priors in our analysis, we constrain at once nine cosmological parameters and four nuisance parameters, which define the relation between cluster mass and X-ray flux. Because of the scale dependence of large-scale bias induced by local-shape non-Gaussianity, we find that the power spectrum provides strong constraints on the non-Gaussianity f_{NL} parameter, which complement the stringent constraints on the power spectrum normalization, σ_8 , from the number counts. To quantify the joint constraints on the two parameters, σ_8 and f_{NL} , that specify the timing of structure formation for a fixed background expansion, we define the figure-of-merit $FoM_{SFT} = (\det [Cov(\sigma_8, f_{NL})])^{-1/2}$. We find that our surveys constrain deviations from Gaussianity with a precision of $\Delta f_{NL} \simeq 10$ at 1σ confidence level, with $FoM_{SFT} \simeq 39$. We point out that constraints on f_{NL} are weakly sensitive to the uncertainties in the knowledge of the nuisance parameters. As an application of non-Gaussian constraints from available data, we analyse the impact of positive skewness on the occurrence of XMMU-J2235, a massive distant cluster recently discovered at $z \simeq 1.4$. We confirm that in a WMAP-7 Gaussian Λ CDM cosmology, within the survey volume, $\simeq 5 \times 10^{-3}$ objects like this are expected to be found. To increase the probability of finding such a cluster by a factor of at least 10, one needs to evade either the available constraints on f_{NL} or on the power spectrum normalization σ_8 .

1 INTRODUCTION

The standard inflationary scenario, based on the single scalar field slow-roll paradigm, predicts primordial density perturbations to be virtually indistinguishable from a Gaussian distribution. However, a number of variants of inflation have been proposed which are able to generate a certain amount of non-Gaussianity (e.g., Bartolo et al. 2004; Chen 2010). Therefore, testing to what precision we can measure possible deviations from Gaussianity with available and future observations has important implications on our understanding of the mechanism that seeded density fluctuations in the early Universe. Analyses of the Cosmic Microwave

Background (CMB) provide at present the tightest constraints on the amount of allowed non-Gaussianity. A number of analyses based on the WMAP data converge to indicate consistency with the Gaussian assumption (e.g., Komatsu et al. 2010 and references therein; cf. also Yadav & Wandelt 2008). While data from the Planck satellite are expected to further tighten such constraints (e.g., Yadav et al. 2007; Liguori et al. 2010), it is worth understanding whether non-Gaussianity can be probed by large-scale structure observations (e.g., Slosar et al. 2008; Verde 2010).

Non-Gaussian perturbations are expected to leave their im-

print also on the pattern of structure growth at least in two different ways. First, we expect that a positively skewed distribution provides an enhanced probability of finding large overdensities. This translates into an enhanced probability of forming large collapsed structures at high redshift, thereby changing the timing of structure formation and the shape and evolution of the mass function of dark-matter halos.

After the first pioneering studies of the effect of non-Gaussianity on the mass function (e.g. Matarrese et al. 1986; Colafrancesco et al. 1989; Borgani & Bonometto 1990), a number of analyses have been carried out since the beginning of 2000s (e.g., Matarrese et al. 2000; Mathis et al. 2004; Kang et al. 2007; Sefusatti et al. 2007; Grossi et al. 2007; Maggiore & Riotto 2009). Furthermore, the realization of large-scale cosmological simulations with non-Gaussian initial conditions have recently provided a validation of the non-Gaussian correction to be applied to the Gaussian mass function (e.g., Grossi et al. 2007; Dalal et al. 2008; Desjacques et al. 2009; Grossi et al. 2009; Giannantonio & Porciani 2009; Pillepich et al. 2010). More recently non-Gaussianity effects on the large-scale distribution of collapsed halos were studied: it has been demonstrated (e.g., Dalal et al. 2008; Matarrese & Verde 2008; Valageas 2010; Lam & Sheth 2009) that non-Gaussianity affects the large-scale clustering of halos in such a way that the linear biasing parameter acquires a scale dependence. This modifies, in a detectable way, the power spectrum of the distribution of any tracer of cosmic structures at small wavenumbers and offers a unique way of testing the nature of primordial fluctuations.

The evolution of the mass function of galaxy clusters identified in X-ray surveys has been extensively used in the past to constrain cosmological models (e.g., Borgani et al. 2001; Rosati et al. 2002; Schuecker et al. 2003; Voit 2005). These studies have recently attracted renewed interest, thanks to detailed follow-up observations of clusters selected from ROSAT observations, they have been carried out either to constrain the Dark Energy equation of state within the Gaussian paradigm (e.g., Vikhlinin et al. 2009; Mantz et al. 2009), or to test possible deviations from standard gravity (e.g., Schmidt et al. 2009; Rapetti et al. 2009). Jimenez & Verde (2009) have recently analyzed the effect of non-Gaussianity on the population of massive high-redshift clusters, like the one recently discovered by Jee et al. (2009) at $z \simeq 1.4$. It is important to remember that the cosmological constraints obtained from clusters so far have been derived from small ROSAT-based samples, containing ~ 100 clusters at $z < 1$. It is therefore easy to imagine the vast margin of improvements offered by next generation X-ray surveys which will detect $\sim 10^5$ clusters to $z \sim 2$.

These surveys should cover a large enough volume at high redshift to test non-Gaussianity in the regimes where its effects are clearer, namely the high-mass tail of the mass function and the large-scale power spectrum of the cluster distribution. Fedeli et al. (2009) and Roncarelli et al. (2010) presented predictions for the number counts and clustering of galaxy clusters expected from the eROSITA X-ray survey and from the Sunyaev–Zeldovich SPT survey. While these analyses confirmed the potential of these surveys to provide interesting constraints on non-Gaussian models, they did not include detailed forecasts on the constraints on non-Gaussian models and a detailed assessment of the effect of uncertainties in the scaling relations between cluster masses and observables. Oguri (2009) followed the self-calibration approach by Lima & Hu (2005) (see also Majumdar & Mohr 2004; Battye & Weller 2003) to forecast the capability of future optical cluster surveys to constrain non-Gaussian models. This study showed that combining

number counts and clustering of galaxy clusters can potentially provide quite strong constraints on deviations from Gaussianity.

The aim of this paper is to derive forecasts, based on the Fisher–Matrix approach, on the capability of future X-ray cluster surveys to constrain deviations from Gaussian perturbations. Besides focusing on the characteristics of X-ray, rather than optically selected samples, our analysis differs from that by Oguri (2009) for the method to include information from large-scale clustering. Oguri (2009) adopted the approach by Lima & Hu (2005) where clustering is included by accounting for fluctuations of cluster counts within cells having a fixed angular size. This implies that, at each redshift, clustering information is restricted to one physical scale. In our analysis, we follow the approach originally presented by Tegmark (1997) (see also Feldman et al. 1994; Majumdar & Mohr 2003), in which the clustering Fisher-Matrix is computed for the allowed range of wavenumbers, by weighting them according to the effective volume covered by the surveys.

Another distinctive aspect of our analysis is that it is based on X-ray surveys of next generation, whose sensitivity and angular resolution are high enough to warrant an accurate measurement of robust mass proxies, related to the cluster gas mass and X-ray temperature for a large number of clusters. As we will discuss in the following, surveys with these characteristics can be provided by an already proposed X-ray telescope, which joins a large collecting area to a large field-of-view and a high angular resolution over the entire field of view (e.g., Giacconi et al. 2009; Vikhlinin et al. 2009). The great advantage of having a similar survey is that there is no need to assume any external follow-up observation for a subset of identified clusters. Moreover, the possibility to define a flux-limit down to which measuring accurate mass proxies for all clusters allows one to set robust priors on the scaling relations between cluster mass and observables, which is one of the main source of uncertainty in the cosmological application of galaxy clusters (e.g., Albrecht et al. 2009).

In principle, the method used in our analysis can be applied to any cluster surveys, including optical and SZ ones. Although so far X-ray surveys have been mostly used for cosmological applications of clusters, upcoming large optical and SZ surveys promise to provide an important contribution to this field. Our method only requires a well defined selection function and calibrated mass proxies. Since cluster surveys at different wavelengths have different efficiencies probing different mass ranges at different redshifts, they will ultimately provide complementary approaches to the derivation of cosmological constraints.

The plan of this paper is as follows. In Section 2 we summarize the formalism to compute non-Gaussian corrections to the mass function and the linear bias parameter of collapsed halos. In Section 3 we describe our approach to compute the Fisher Matrix for both the number counts and the power spectrum of galaxy clusters. In Section 4 we first describe how we compute the selection function and the redshift distribution expected for the X-ray surveys, then we present the results in terms of constraints on the parameter space defined by the non-Gaussianity parameter, f_{NL} , and the power spectrum normalizations, σ_8 . Section 5 is devoted to the discussion of these results. In this section we will also discuss the competing effects of non-Gaussianity and normalization of the power spectrum on the expected number of clusters at $z > 1.4$, which have a mass of, at least, $5 \times 10^{14} M_\odot$, as the one recently studied by Jee et al. (2009). We summarize our main conclusions in Section 6.

2 NON-GAUSSIAN INITIAL CONDITIONS

Generalizations of the most standard model of inflation (Guth 1981) give rise to seed primordial density fluctuations that follow a non-Gaussian probability distribution (e.g., Bartolo et al. 2004; Chen 2010, for reviews). A particularly convenient way to parametrize the deviation of this distribution from the Gaussian one consists of writing the Bardeen's gauge invariant potential Φ as the sum of a linear Gaussian term and a quadratic correction (Salopek & Bond 1990; Gangui et al. 1994; Verde et al. 2000; Komatsu & Spergel 2001),

$$\Phi = \Phi_G + f_{NL} * (\Phi_G^2 - \langle \Phi_G^2 \rangle). \quad (1)$$

In Eq. (1), the symbol $*$ denotes convolution between functions and reduces to simple multiplication only in the particular case of constant f_{NL} , while in general it is a function of the scale. Note that on scales smaller than the Hubble radius the function Φ equals minus the Newtonian peculiar gravitational potential. The fundamental parameter f_{NL} denotes the amplitude of the deviation from Gaussianity, and is related to the skewness of the distribution (see below).

We adopt, in the following, the Large Scale Structure convention (as opposed to the CMB convention, see Afshordi & Tolley 2008; Pillepich et al. 2010; Carbone et al. 2008; Grossi et al. 2009) for defining the parameter f_{NL} . This means, among other things, that the constraints given on f_{NL} by the CMB have to be raised, according to the linear growth of structures, as $f_{NL} = g(+\infty)f_{NL}^{\text{CMB}}/g(0) \simeq 1.3f_{NL}^{\text{CMB}}$, where $g(z)$ is the linear growth suppression factor with respect to the Einstein-de Sitter cosmology.

If the distribution of primordial density (and potential) perturbations is not Gaussian, it cannot be fully described by a power spectrum expressed as $P_\Phi(\mathbf{k}) = Bk^{n-4}$ (where $k = \|\mathbf{k}\|$), but we need higher-order moments such as the bispectrum $B_\Phi(\mathbf{k}_1, \mathbf{k}_2, \mathbf{k}_3)$. In particular, different models of inflation give rise to different shapes of the bispectrum. In the following we adopt one particular shape, called *local shape*, means that the bispectrum is maximized for configurations in which one of the three momenta is much smaller than the other two ("squeezed" configurations). Inflationary models exist that produce different shapes for the primordial bispectrum, e.g., the *equilateral shape* (see Crociani et al. 2009; Fedeli et al. 2009 for applications), or the *enfolded shape* (Holman & Tolley 2008; Meerburg et al. 2009; Verde & Matarrese 2009), however, the local shape is the one giving the largest effects especially on bias (Fedeli et al. 2009; Taruya et al. 2008), hence we limit our analysis to this case only.

In this case the parameter f_{NL} is a dimensionless constant and the bispectrum can be written as (e.g., Creminelli et al. 2007; LoVerde et al. 2008)

$$B_\Phi(\mathbf{k}_1, \mathbf{k}_2, \mathbf{k}_3) = 2f_{NL}B^2 \left[k_1^{n-4}k_2^{n-4} + k_1^{n-4}k_3^{n-4} + k_2^{n-4}k_3^{n-4} \right], \quad (2)$$

where n is the primordial spectral index and B is the amplitude of the spectrum $P_\Phi(\mathbf{k})$, related to the amplitude A of the power spectrum of density fluctuations, $P(k) = Ak^n$, by the relation

$$B = \frac{9}{4}AH_0^4\Omega_{m,0}^2. \quad (3)$$

Two of the ingredients that critically affect the observed properties of the cluster population are influenced by non-Gaussian initial conditions: the halo mass function and the linear bias of dark-matter halos.

2.1 Mass function

For the mass function of cosmic structures in non-Gaussian cosmologies different prescriptions exist. The one adopted here is taken from LoVerde et al. (2008), where the authors approximated the probability distribution for the smoothed dark-matter density field using the Edgeworth expansion and then performed the integral of the probability distribution for threshold crossing exactly on the first few terms of the expansion itself. The result for the Press & Schechter (1974) (PS) mass function reads

$$\begin{aligned} n_{NG}(M, z) = & -\sqrt{\frac{2}{\pi}} \frac{\bar{\rho}}{M} \exp \left[-\frac{\delta_c^2(z)}{2\sigma_M^2} \right] \left[\frac{d \ln \sigma_M}{dM} \left(\frac{\delta_c(z)}{\sigma_M} + \right. \right. \\ & + \frac{S_3 \sigma_M}{6} \left(\frac{\delta_c^4(z)}{\sigma_M^4} - 2 \frac{\delta_c^2(z)}{\sigma_M^2} - 1 \right) \left. \right) + \\ & \left. + \frac{1}{6} \frac{dS_3}{dM} \sigma_M \left(\frac{\delta_c^2(z)}{\sigma_M^2} - 1 \right) \right]. \end{aligned} \quad (4)$$

In Eq. (4) $\delta_c(z) \equiv \Delta_c/D(z)$, where $D(z)$ is the linear growth factor, σ_M is the *rms* of primordial density fluctuations on the scale corresponding to mass M , while $S_3(M) \equiv f_{NL}\mu_3(M)/\sigma_M^4$ is the normalized skewness. The third-order moment $\mu_3(M)$ can be written as

$$\mu_3(M) = \int_{\mathbb{R}^9} \mathcal{M}_R(k_1) \mathcal{M}_R(k_2) \mathcal{M}_R(k_3) B_\Phi(\mathbf{k}_1, \mathbf{k}_2, \mathbf{k}_3) \frac{d\mathbf{k}_1 d\mathbf{k}_2 d\mathbf{k}_3}{(2\pi)^9}. \quad (5)$$

The function $\mathcal{M}_R(k)$ relates the Fourier transform of density fluctuations smoothed on some scale R to the relative peculiar potential, and is defined as

$$\mathcal{M}_R(k) \equiv \frac{2}{3} \frac{T(k)k^2}{H_0^2 \Omega_{m,0}} W_R(k), \quad (6)$$

where $T(k)$ is, in our analysis, the matter transfer function (Eisenstein & Hu 1998) and $W_R(k)$ is the top-hat window function. Eq. 4 gives the correction to the PS mass function. However, we know that the PS mass function provides only an approximate fit to the results of N-body simulations. The commonly adopted procedure is then to assume that the same correction appearing in Eq. (4) can be applied to the best-fit Gaussian mass function to derive an accurate expression for the non-Gaussian one:

$$n(M, z) = n_{(G)}(M, z) \frac{n_{NG}(M, z)}{n_{PS}(M, z)}. \quad (7)$$

Here $n_{(G)}(M, z)$ is the mass function in the reference Gaussian model computed according to the Sheth & Tormen (2002) recipe, while $n_{NG}(M, z)$ and $n_{PS}(M, z)$ represent the Press & Schechter (1974) mass functions in the non-Gaussian (Eq. 4) and reference Gaussian model respectively.

As already discussed, different prescriptions can be found in the literature that give different expressions for the mass function in non-Gaussian models. For instance, Matarrese et al. (2000) used the saddle point approximation to compute the probability distribution of threshold crossing, and then truncated the resulting expression to the skewness. The resulting mass function is however in agreement with the one obtained by LoVerde et al. (2008), as are the other recipes found in the literature.

Grossi et al. (2009) have shown that these analytic expressions are in agreement with N-body cosmological simulations, provided the linear threshold for collapse is corrected for ellipsoidal density perturbations, according to $\Delta_c \rightarrow \Delta_c \sqrt{q}$, with $q = 0.75$. We adopted this correction in our calculations.

2.2 Bias

The halo bias acquires an extra scale dependence due to primordial non-Gaussianity, that can be written as (Matarrese & Verde 2008)

$$b(M, z, k) = b^{(G)}(M, z) + \Delta b(M, z, k), \quad (8)$$

where

$$\Delta b(M, z, k) = [b^{(G)}(M, z) - 1] \delta_c(z) \Gamma_R(k). \quad (9)$$

The term $\Gamma_R(k)$ encapsulates the dependence on the scale and on the mass, and can be written for a local bispectrum shape as

$$\begin{aligned} \Gamma_R(k) = & \frac{2f_{NL}}{8\pi^2 \mathcal{M}_R(k) \sigma_R^2} \int_0^{+\infty} d\zeta \zeta^2 \mathcal{M}_R(\zeta) P_\Phi(\zeta) \times \\ & \times \left\{ \int_{-1}^1 d\mu \mathcal{M}_R(\sqrt{\alpha}) \left[\frac{P_\Phi(\sqrt{\alpha})}{P_\Phi(k)} + 2 \right] \right\}, \end{aligned} \quad (10)$$

where $\alpha = \zeta^2 + k^2 + 2\mu\zeta k$. The linear bias in the reference Gaussian model can be written as

$$\begin{aligned} b^{(G)}(M, z) = & 1 + \frac{a\Delta_c}{D^2(z)\sigma_M^2} - \frac{1}{\Delta_c} + \\ & + \frac{2p}{\Delta_c} \left[\frac{(D(z)\sigma_M)^{2p}}{(D(z)\sigma_M)^{2p} + (\sqrt{a}\Delta_c)^{2p}} \right], \end{aligned} \quad (11)$$

according to the prescriptions of Mo & White (1996); Sheth & Tormen (1999); Sheth et al. (2001), and with parameters set to $p = 0.3$ and $a = 0.75$.

In order to obtain agreement with the results of numerical simulations it is necessary to correct the linear overdensity for collapse, this time according to $\Delta_c \rightarrow \Delta_c q$ with $q = 0.75$ (Grossi et al. 2009). Semi-analytic results, with this correction, are also in agreement with the numerical results of Pillepich et al. (2010) (see also Desjacques et al. 2009). We adopted this correction in the remainder of our calculations. For figures showing the scale, mass and redshift dependence of this correction to the linear bias we refer to Taruya et al. (2008) and Fedeli et al. (2009).

3 FISHER MATRIX ANALYSIS

The Fisher Matrix formalism can be used to understand how accurately we can estimate the values of a vector of parameters \mathbf{p} for a given model from one or more data sets, under the assumption that all parameters follow a Gaussian distribution (e.g., Cash 1979).

The information Fisher Matrix (FM hereafter) is defined as

$$F_{\alpha\beta} \equiv - \left\langle \frac{\partial^2 \ln \mathcal{L}}{\partial p_\alpha \partial p_\beta} \right\rangle, \quad (12)$$

where \mathcal{L} is the likelihood of an observable (in our case the number of galaxy clusters in a given redshift and mass range or the averaged power spectrum of the cluster distribution).

3.1 Number counts

Following the approach of Holder et al. (2001) and Majumdar & Mohr (2003), the Fisher matrix for the number of clusters, $N_{l,m}$, within the l -th redshift bin and m -th bin in observed mass M^{ob} , can be written as

$$F_{\alpha\beta}^N = \sum_{l,m} \frac{\partial N_{l,m}}{\partial p_\alpha} \frac{\partial N_{l,m}}{\partial p_\beta} \frac{1}{N_{l,m}}, \quad (13)$$

where the sums over l and m run over redshift and mass intervals, respectively. With this notation, it is $M_{l,m=0}^{ob} = M_{\text{thr}}(z)$, where $M_{\text{thr}}(z)$ is defined as the threshold value of the observed mass for a cluster to be included in the survey. Due to the selection function of any X-ray flux-limited survey, the value of $M_{\text{thr}}(z)$ depends on redshift (see Section 4.1). Therefore, the number of mass bins and their extent in our analysis will change with redshift accordingly.

We write the number of clusters expected in a survey having a sky coverage $\Delta\Omega$ with observed mass between $M_{l,m}^{ob}$ and $M_{l,m+1}^{ob}$ and redshift between z_l and z_{l+1} as

$$\begin{aligned} N_{l,m} = & \Delta\Omega \int_{z_l}^{z_{l+1}} dz \frac{dV}{dz d\Omega} \int_{M_{l,m}^{ob}}^{M_{l,m+1}^{ob}} dM^{ob} \\ & \int_0^\infty dM n(M, z) p(M^{ob} \mid M). \end{aligned} \quad (14)$$

In the above equation dV/dz is the cosmology-dependent comoving volume element per unity redshift interval and solid angle, $n(M, z)$ the mass function, i.e. the number density of clusters with true mass M at redshift z (see Section 2.1).

As already mentioned, we assume in the following the expression by Sheth & Tormen (1999) for the Gaussian halo mass function. We remind here that other calibrations of the halo mass function from simulations have been presented by several authors (e.g., Jenkins et al. 2001; Warren et al. 2006; Tinker et al. 2008; Crocce et al. 2010). While using the best-calibrated mass function is in fact important when deriving cosmological constraints from real data (e.g., Wu et al. 2010), it has only a minor impact when deriving forecasts on cosmological constraints. Indeed, what matters for the latter is the total number of clusters expected in a given cosmological model, which is far more sensitive to the choice of reference cosmological and nuisance parameters than to the details of the mass function fitting function.

Following Lima & Hu (2005) we assign to each cluster with true mass M a probability $p(M^{ob} \mid M)$ of having an observed mass M^{ob} , as inferred from a given mass proxy. Under the assumption of a log-normal distribution for the intrinsic scatter in the relation between true and observed mass, with variance $\sigma_{\ln M}^2$, the expression for the probability is

$$p(M^{ob} \mid M) = \frac{\exp[-x^2(M^{ob})]}{\sqrt{(2\pi\sigma_{\ln M}^2)}}, \quad (15)$$

where

$$x(M^{ob}) = \frac{\ln M^{ob} - B_M - \ln M}{\sqrt{(2\sigma_{\ln M}^2)}}. \quad (16)$$

Here we allow the relation between true and observed mass to be characterized not only by an intrinsic scatter, but also by a systematic bias in the mass estimate, whose fractional value is given by B_M . By inserting Eq.(15) into Eq.(14) for the cluster counts in a given mass and redshift interval, we obtain

$$\begin{aligned} N_{l,m} = & \frac{\Delta\Omega}{2} \int_{z_l}^{z_{l+1}} dz \frac{dV}{dz d\Omega} \int_0^\infty dM n(M, z) \\ & \times [\text{erfc}(x_m) - \text{erfc}(x_{m+1})] \end{aligned} \quad (17)$$

with $x_m = x(M_{l,m}^{ob})$ and $\text{erfc}(x)$ the complementary error function. We note that the possibility of factorising the sky-coverage outside the integration relies on the assumption that clusters in our survey are detected over the same area of the sky down to the survey completeness limit. The above expression can be easily generalized to include the possibility of a “flux”-dependent sky coverage.

We remark that we neglect clustering contribution to the noise (i.e. cosmic variance). Indeed, the Wide and the Medium surveys (see Table 1) covers large enough area over which cosmic variance is negligible. This may not be case for the Deep survey, which however, as we shall see, does not bring much cosmological constraints (see Section 4.1).

3.2 Power spectrum

In order to include in our analysis the information from the clustering of galaxy clusters, we follow the approach by Majumdar & Mohr (2004). We define the Fisher Matrix for the power spectrum of galaxy clusters as

$$F_{\alpha\beta} = \frac{1}{(2\pi)^2} \sum_{l,m} \frac{\partial \ln \bar{P}_{cl}(k_m, z_l)}{\partial p_\alpha} \frac{\partial \ln \bar{P}_{cl}(k_m, z_l)}{\partial p_\beta} V_{l,m}^{eff} k_m^2 \Delta k, \quad (18)$$

where the sums in l and m run over redshift and wavenumber k bins, respectively (Tegmark 1997; Feldman et al. 1994). In the above equations \bar{P}_{cl} is the average cluster power spectrum calculated within the given redshift interval,

$$\bar{P}_{l,m}^{cl}(k, z_i) = \frac{\int_{z_l}^{z_{l+1}} dz \frac{dV}{dz} N^2(z) P^{cl}(k, z)}{\int_{z_l}^{z_{l+1}} dz \frac{dV}{dz} N^2(z)}. \quad (19)$$

This amounts to weight the cluster power spectrum, $P^{cl}(k, z)$, according to the square of the number density of clusters, $N(z)$, that are included in the survey at redshift z . In turn, the cluster power spectrum $P^{cl}(k, z)$ is expressed in terms of power spectrum, $P(k, z)$, of the cosmic density fluctuations according to $P^{cl}(k, z) = b_{eff}^2(k, z) P(k, z)$; here the effective bias is defined as the linear bias, introduced in Sect. 2, weighted by the mass function,

$$b_{eff}(z, k) = \frac{\int_0^\infty dM n(M, z) \operatorname{erfc}[x(M_{thr})] b(M, z, k)}{\int_0^\infty dM n(M, z) \operatorname{erfc}[x(M_{thr})]}. \quad (20)$$

The bias parameter $b(M, z, k)$ acquires the dependence on the wavenumber k predicted by non-Gaussian models (see Sect. 2.2). Finally, the quantity $V^{eff}(k, z)$ in Eq.(18) is the effective volume accessible by the survey at redshift z at wavenumber k . This effective volume is weighted by the shot noise level $1/N(z)$, so that

$$V^{eff}(k, z) = V_0(z) \left[\frac{N(z) \bar{P}_{cl}(k, z)}{1 + N(z) \bar{P}_{cl}(k, z)} \right]^2, \quad (21)$$

with $V_0(z)$ the total comoving volume covered by the redshift bin centred on z . In this way, constraints at redshift z are mostly contributed by wavemodes k , which maximize $N(z) \bar{P}_{cl}(k, z)$ and make V^{eff} approach V_0 .

An alternative approach to include clustering information in deriving FM survey forecasts has been proposed by Lima & Hu (2005) and applied also by Oguri (2009) for constraints on non-Gaussian models from cluster surveys. In this approach, one makes a partition of the sky area covered by a survey into regular cells of a fixed angular size and then computes the fluctuations in the cluster counts within such cells. Since this method does not explicitly include the covariance between counts within different cells, it only samples clustering at a fixed angular scale (i.e. at a single physical scale for a fixed redshift). On the other hand, extracting the full information content in the scale dependence of the power spectrum is quite important when constraining non-Gaussian models, whose unique signature is given by the scale-dependent bias. Cunha et al. (2010) used the count-in-cell approach by also including the information from the covariance. Therefore, the information on the

large-scale power spectrum, in the count-in-cell approach, is conveyed by the covariance terms. In our approach the different scales are weighted by the effective volume, defined by Eq.(21).

In our analysis we assume the following reference values for the cosmological parameters, consistent with the WMAP-7 best-fitting model (Komatsu et al. 2010): $\Omega_m = 0.28$ for the present-day matter density parameter, $\sigma_8 = 0.81$ for the normalization of the power spectrum, $\Omega_k = 0$ for the contribution from the curvature, $w(a) = w_0 + (1 - a) w_a$ with $w_0 = -0.99$ and $w_a = 0$ for the Dark Energy equation of state, $\Omega_b = 0.046$ for the contribution of baryons to the density parameter, $h = 0.70$ for the Hubble parameter, $n = 0.96$ for the primordial spectral index and $f_{NL} = 0$ for the non-Gaussianity parameter. Therefore, we have in total 9 cosmological parameters, which are left free to vary in the computation of the number counts and power spectrum Fisher Matrices of Eqs.(13) and (18).

In the following, all the results presented are based on adding the Fisher Matrix for the Planck CMB experiment to those from the cluster surveys. We derive the cosmological constraints from Planck following the description laid out by the DETF Albrecht et al. (2009) and use the method described in Rassat et al. (2008). We conservatively assume that we will only use the 143 GHz channel as science channel. This channel has a beam of $\theta_{\text{fwhm}} = 7.1'$ and sensitivities of $\sigma_T = 2.2\mu K/K$ and $\sigma_P = 4.2\mu K/K$. We take $f_{\text{sky}} = 0.80$ as the sky fraction in order to account for galactic foregrounds. We use as a minimum ℓ -mode, $\ell_{\min} = 30$ in order to avoid problems with polarization foregrounds. As described in the DETF report (Albrecht et al. 2009) we choose as fiducial parameter set $\theta = (\omega_m, \theta_S, \ln A_S, \omega_b, n_S, \tau)$, where θ_S is the angular size of the sound horizon at last scattering, $\ln A_S$ is the logarithm of the primordial amplitude of scalar perturbations and τ is the optical depth due to reionization. After marginalization over the optical depth we then calculate the Planck CMB Fisher matrix in the parameters $(\Omega_m, \Omega_{de}, h, \sigma_8, \Omega_b, w_0, w_a, n_S)$ by using the appropriate Jacobian of the involved parameter transformation (Rassat et al. 2008). We point out that the Planck FM is computed for Gaussian perturbations. Therefore, while it adds quite strong constraints on the other cosmological parameters, especially on the curvature, it does not add any constraints on f_{NL} .

4 ANALYSIS AND RESULTS

4.1 Characteristics of the surveys

The commonly adopted procedure to estimate cosmological forecasts for X-ray surveys is based on calibrating a flux limit for cluster detection (which generally corresponds to the detection of few tens of net photon counts in an extended source), and to use fluxes as proxies to cluster masses. In order to account for the uncertain knowledge of the relation between X-ray luminosity and mass, several authors have proposed to follow the so-called self-calibration method (e.g., Majumdar & Mohr 2003, 2004; Lima & Hu 2004, 2005). In this approach the relation between mass and observable is defined up to an intrinsic scatter, also including the possibility of a systematic bias in the estimate of cluster masses. The parameters defining the relation between mass and observable are then treated as fitting ‘‘nuisance’’ parameters to be determined along with the relevant cosmological parameters.

An alternative approach, adopted to derive cosmological constraints from cluster surveys, is, instead, based on restricting the analysis to a relatively small subset of galaxy clusters for which

Table 1. Characteristics of the X-ray surveys (see also Giacconi et al. 2009). Column 2: sky coverage Ω (in sq.deg.); Column 3: flux limits for detection of extended sources in the [0.5–2] keV energy band (units of 10^{-14} erg s $^{-1}$ cm $^{-2}$); Column 4: flux limits defining the *bright* subsamples (see text).

	Ω	F_{det}	F_{br}
Wide	20000	0.5	15.0
Medium	3000	0.1	3.0
Deep	100	0.01	0.3

deeper X-ray follow-up observations provide measures of mass proxies which are more closely related to cluster masses (e.g., Vikhlinin et al. 2009; Mantz et al. 2009). Examples of such robust mass proxies are the so-called $Y_X = M_{\text{gas}} T_X$, defined as the product of gas mass and temperature at a given radius (e.g., Kravtsov et al. 2006), or M_{gas} itself. They are robust in the sense that, based on simulations, their relation with cluster mass has an intrinsic scatter of 10 per cent or less, especially when emission from cluster cores can be resolved and/or removed. While having obvious advantages, the limitation of relying on such low-scatter mass proxies is that they can be measured for a relatively small number of clusters. In this sense, one has to compromise between the requirement to keep under control the systematics in mass measurements and the need to cover a relatively large redshift baseline with adequate statistics.

Ideally, one should carry out an X-ray survey at such a good sensitivity that low-scatter mass proxies can be measured in survey mode for a large number of galaxy clusters. This would allow an “educated” self-calibration analysis of the cluster surveys, in which the systematics in mass measurements can be kept under control.

In the following, we derive forecasts for three X-ray surveys, which are complementary in terms of sensitivity and sky coverage, inspired to the survey strategy devised for the Wide Field X-ray Telescope (WFXT¹), recently proposed to the Astro-2010 Decadal Survey panel (e.g., Murray & WFXT Team 2010; Giacconi et al. 2009; Vikhlinin et al. 2009). This telescope combines a large collecting area and field of view with a sharp PSF over the entire field of view. Thanks to these characteristics, the WFXT has the potential of detecting a large number of clusters out to $z \sim 2$ and of measuring Y_X or M_{gas} with good precision down to relatively low fluxes. While describing the characteristics of the WFXT is outside the scope of this paper, we point out that such an instrument would have the capability of measuring low-scatter mass proxies down to cluster fluxes which are comparable to fluxes at which clusters are just detected in current and future X-ray telescopes. Based on the results presented by Giacconi et al. (2009), we give in Table 1 the limiting fluxes (in the 0.5–2 keV energy band) at which WFXT will detect a cluster as an extended source in three surveys: a Wide Survey, which will cover all the extragalactic sky (20000 deg 2) with a sensitivity ~ 500 times better than the ROSAT All Sky Survey (e.g., Voges et al. 1999); a Medium Survey, which will reach over 3000 deg 2 flux limits comparable to those of the deep Chandra and XMM deep COSMOS fields (Cappelluti et al. 2009); a Deep Survey that will reach over 100 deg 2 a sensitivity similar to those of the deepest Chandra pointings. Thanks to the large collecting area and field of view of WFXT, and taking advantage of its good angular resolution (5 arcsec half energy width, approximately constant over the whole field-of-view), these surveys could be completed within a five-year mission duration (Murray & WFXT Team 2010).

¹ <http://www.eso.org/~prosati/WFXT/Overview.html>, <http://wfxt.pha.jhu.edu/>

In principle, a unique flux limit is not sufficient to define a completeness criterion in an X-ray survey. In fact, due to vignetting and PSF variation with off-axis angle, the flux limit for the detection of a source at a given signal-to-noise varies across the field of view. For this reason, rather than a flux limit, one should calibrate a flux-dependent sky coverage. Owing the approximate uniformity of the WFXT PSF, we expect such a sky coverage to be quite steep around the flux limits reported in Table 1, so that we ignore its flux-dependence in the following analysis. In order to convert these flux limits into mass limits, we use the relation between X-ray luminosity and M_{500} calibrated by Maughan (2007), where masses are recovered from Y_X , using Chandra data for 115 clusters in the redshift range $0.1 < z < 1.3$. Among the fitting expressions reported in Table 1 of that paper, we choose the relation between L_X and M_{500} , obtained without excising the core region within $0.15 R_{500}$:

$$L_X = C E(z) \left(\frac{M_{500}}{4 \times 10^{14} M_{\odot}} \right)^B, \quad (22)$$

with $C = 5.6$, $B = 1.96$.

The reason for this choice is that we did not attempt to model the core contribution in computing the flux limits reported in Table 1.

We show in Figure 1 the redshift dependence of the limiting mass² M_{500} associated to the survey flux limits. The value of the virial mass, which is the relevant quantity entering in the mass function choosed in our analysis, is obtained from M_{500} , following Hu & Kravtsov (2003), by adopting the NFW halo density profile (Navarro et al. 1997) for the reference cosmological model, assuming $c = 5$ for the concentration parameter (see also Shang et al. 2009). Also shown in Figure 1 with the green short-dashed curve is the mass limit corresponding to a flux 30 times brighter than the flux limit for cluster detection in the Deep Survey. Since cluster detection in the Deep survey corresponds to about 200 net counts, such a mass limit is for clusters for which about 6000 counts would be available. With such a large number of counts one has a precise measurement of robust mass proxies such as Y_X and M_{gas} . We point out that clusters identified in the Deep Survey allows one to calibrate mass proxies down to fluxes which are lower than the flux for cluster identification in the Wide Survey. Such brighter flux limits define the *bright samples* of clusters, for which a direct measurement of a mass proxy can be carried out within the same surveys. Extrapolating the $M-L_X$ relation by Maughan (2007) at faint fluxes of our surveys would imply unrealistically small mass limits at low redshift. For this reason, we decided to use a lower limit of $M_{500} = 5 \times 10^{13} h^{-1} M_{\odot}$ in the definition of the selection function (shown with the horizontal dotted line in Figure 1). In fact, this is comparable to the lowest mass down to which mass proxies have been calibrated so far (e.g., Vikhlinin et al. 2009). We also point out that, for the sake of simplicity, we do not include the cosmology dependence of the selection function in our analysis.

4.2 Nuisance parameters

Besides the nine cosmological parameters, our FM analysis should also constrain the nuisance parameters which specify the redshift dependence of the fraction mass bias B_M and the intrinsic scatter $\sigma_{\ln M}$ (in our analysis we do not consider the case of a possible

² Here and in the following we indicate with M_{Δ} the mass contained within the radius R_{Δ} , encompassing an average density of Δ times the critical cosmic density ρ_{cr} .

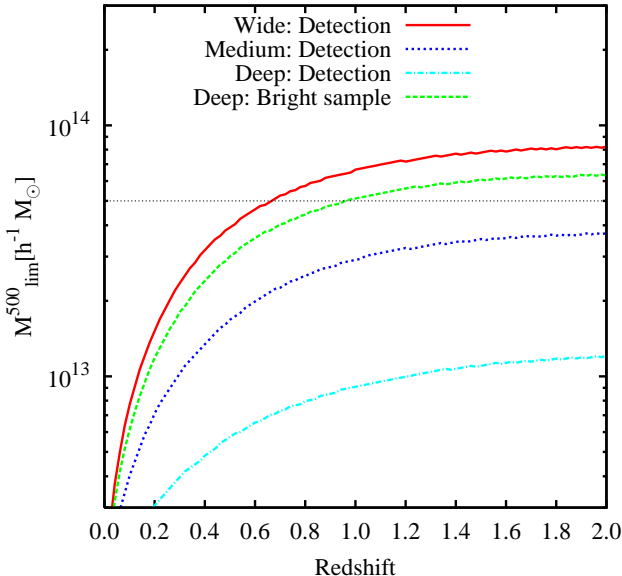


Figure 1. The redshift dependence of the M_{500} mass thresholds, corresponding to the flux limits for cluster detection for the three surveys, as reported in Table 1: the Wide, Medium and Deep surveys are shown with the solid (red), the dotted (blue) and dot-dashed (cyan) curves, respectively. The short-dashed (green) curve corresponds to a flux-limit which is 30 times brighter than the flux limit for cluster detection in the Deep survey. The horizontal dotted line marks the mass limit of $M_{500} = 5 \times 10^{13} h^{-1} M_{\odot}$ below which we discard clusters in our analysis.

mass dependence of these parameters). According to Lima & Hu (2005), we assume the following parametrization for such redshift dependencies:

$$\begin{aligned} B_M(z) &= B_{M,0}(1+z)^\alpha \\ \sigma_{\ln M}(z) &= \sigma_{\ln M,0}(1+z)^\beta. \end{aligned} \quad (23)$$

In this way, we have four nuisance parameters, $B_{M,0}$, $\sigma_{\ln M,0}$, α and β . A negative value for B_M corresponds to a mass underestimate and, therefore, to a smaller number of clusters included in a survey, for a fixed selection function. The presence of the mass bias accounts for the possibility of a violation of hydrostatic equilibrium in the estimate of X-ray masses, on which the observable-mass scaling relation is calibrated. A number of independent analyses of a variety of cosmological hydrodynamic simulations of galaxy clusters converge to indicate that hydrostatic mass estimators provide underestimates of true mass within R_{500} by about 10–15 per cent (e.g., Rasia et al. 2005; Nagai et al. 2007; Ameglio et al. 2009; Piffaretti & Valdarnini 2008). Quite reassuringly, such results also agree with the observational results on the comparison between cluster masses estimated with weak lensing and with X-ray data (e.g., Mahdavi et al. 2008). In the following we assume $B_{M,0} = -0.15$ as a reference value for the mass bias and regarding its evolution, we take $\alpha = 0$ as a reference value. As for the intrinsic scatter, it has the effect of increasing the number of clusters included in the survey. In fact, the number of low-mass clusters that are up-scattered above the survey mass limit is always larger than the number of rarer high-mass clusters which are down-scattered below the same mass limit (e.g., Cunha 2009, and references therein). As a reference value, we assume $\sigma_{\ln M,0} = 0.25$, consistent with the intrinsic scatter in the $M_{500}-L_X$ relation measured by Maughan (2007), with $\beta = 0$ for its evolution. We stress here that, following Lima & Hu (2005), we use the variance $\sigma_{\ln M}^2$

and not the scatter as the parameter to be varied in our Fisher matrix analysis. In fact, this quantity controls the excess of up-scattered and down-scattered clusters with respect to the total number.

In the following we will not assume any prior for these four nuisance parameters in our reference analysis. We will refer to it as the *no prior* analysis.

On the other hand, already available data allow one to set constraints on the value of the mass bias from the comparison between X-ray and lensing cluster mass measurements. For instance, Vikhlinin et al. (2009) compared weak lensing and Chandra X-ray mass measurements for a rather small sample of low- z clusters and concluded that the mass scale can already be calibrated with a statistical uncertainty of about 10 per cent. A similar result has been obtained by Zhang et al. (2010) from the comparison of XMM-Newton X-ray masses and weak lensing masses for a set of 12 nearby clusters. Owing to these results, we also consider the case of the mass bias parameter to be known with a precision $\Delta B_{M,0} = 0.05$. An improvement by only a factor of two with respect to the present in the calibration of the cluster mass scale is probably overconservative, owing to the orders-of-magnitude increase in the number of clusters with precise X-ray mass measurements to be provided by the three surveys and precise lensing mass measurements from both ground-based and space telescopes. As for the evolution, we assume $\Delta\alpha = 1$ as a prior, which would correspond to an uncertainty in the mass bias calibration at $z = 1$ comparable to that calibrated at present for nearby clusters. Regarding the prior on the intrinsic scatter, we assume $\Delta\sigma_{\ln M,0} = 0.1$ and $\Delta\beta = 1$. We expect these to be rather conservative choices, in view of the large number of clusters that should be made available by future X-ray and optical/near-IR surveys at both low and high redshift. In the following, we refer to these choices of the priors for the nuisance parameters as the *weak prior* analysis.

Finally, we also refer to the *strong prior* analysis for the case in which nuisance parameters are assumed to be known with little uncertainty and are thus kept fixed to their reference values. While this assumption is expected to be unrealistic for fluxes reaching the limiting flux for cluster detection in the three surveys, it may be rather plausible in case we restrict the analysis to the *bright* subsamples.

While we use the *no prior* choice as a reference for the analysis of the surveys down to the detection limit, we will show how much we would gain in terms of constraining power by using instead the *weak prior* and the *strong prior* assumptions. Finally, we will present results for the *bright* surveys for the case of *strong priors* on the nuisance parameters. This will allow us to judge the trade-off between having statistically richer (i.e. lower flux limit) surveys with a less controlled calibration of the cluster mass-luminosity conversion, and a brighter flux limit with better controlled nuisance parameters.

As a first check, we verify that our reference model provides a good fit to present data. We show in Figure 2 the comparison between the cluster flux number counts observed in the [0.5–2] keV energy band from the ROSAT Deep Cluster Survey (Rosati et al. 1998, 2002) and the prediction of our reference model. This is not surprising, owing to the fact that the reference cosmological parameters agree with constraints based on the evolution of the cluster mass function (e.g., Borgani et al. 2001; Vikhlinin et al. 2009; Mantz et al. 2009). The good agreement between available observational data and predictions of our reference model indicates that the latter can be used to provide a realistic extrapolation of the evo-

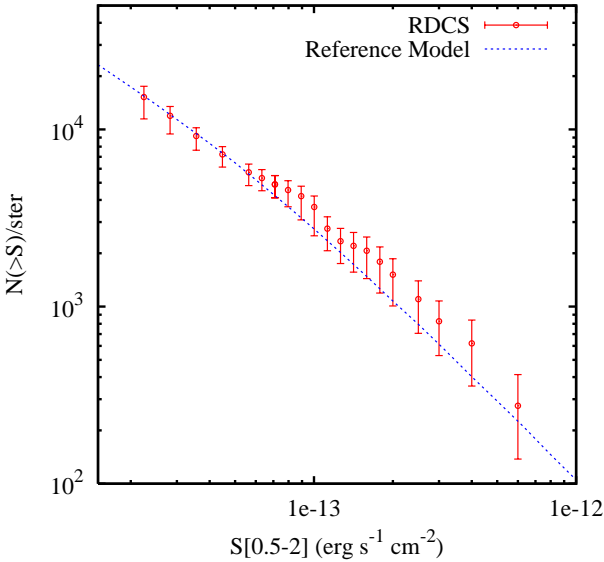


Figure 2. The comparison between observed cumulative cluster flux number counts (symbols with errorbars) and predictions from the reference model (dotted curve, see text). Observational results refer to counts in the [0.5-2] keV band from the ROSAT Deep Cluster Survey (Rosati et al. 2002), with errorbars corresponding to 1σ Poissonian uncertainties.

lution of the cluster mass function over redshift and mass ranges which are not probed by currently available data.

We show in Figure 3 the cumulative redshift distributions for the clusters to be detected in the three surveys (left panel) and for the *bright samples* (right panel). Overall, the three WFXT surveys would yield about 3×10^6 detected clusters, out of which $\sim 7.5 \times 10^4$ clusters should be found at $z > 1$. This will provide an improvement by about four orders of magnitude with respect to the ~ 10 $z > 1$ clusters currently confirmed. At the same time, we expect to have about 2×10^4 clusters with robustly measured mass proxies, of which ~ 4000 would lie at $z > 0.5$. This would increase by more than two orders of magnitude the number of clusters for which mass proxies have been measured above this redshift, after intensive follow-up Chandra observations of clusters identified in ROSAT-based surveys (e.g., Vikhlinin et al. 2009; Mantz et al. 2009; Ettori et al. 2009). We stress that, despite the small area covered, the Deep survey provides the dominant contribution to the *bright sample* at $z > 1$. This highlights the important role that the Deep survey has in providing mass proxies at high redshift. Although predicting the number of extremely distant clusters is highly uncertain, owing to the unknown evolution of the mass luminosity relation above $z \simeq 1$, we foresee that $\sim 10^3$ clusters would be detected at $z \gtrsim 2$, with mass measurements available for few tens of them. In order to quantify the increase in sensitivity provided by the WFXT surveys with respect to currently planned X-ray missions, we computed the redshift distributions expected for the surveys to be carried out by the eROSITA satellite³. In the three years of operation eROSITA is expected to find, for our reference model, $\simeq 4000$ clusters at $z > 1$, while virtually no clusters with precise measurements of mass proxies would be found at $z > 0.5$ in the *bright surveys* having flux limits 30 times higher than for detection.

An important lesson learned from the Chandra follow-up ob-

servations of distant clusters is the fundamental relevance of a sharp PSF to excise the contribution of cool cores in the measurements of mass proxies. Indeed, as shown by a number of authors (e.g., Maughan 2007; Pratt et al. 2010), excising the core contribution suppresses by a substantial amount the intrinsic scatter in the relation between cluster X-ray observables and masses. The sharp PSF with which the WFXT would carry out the surveys, should guarantee a good control of the cool core contribution in the calibration of mass proxies, even to $z \sim 1.5$ without the need of follow-up observations with other higher resolution X-ray telescopes. We also emphasize that a sharp PSF, such that expected for WFXT, has the additional benefit of easing the subtraction of the point source contribution when measuring cluster fluxes. This allows an accurate assessment of the survey flux completeness.

4.3 Constraints on non-Gaussianity

Having defined the reference cosmological model and mass-flux conversion, we present now forecasts on constraints from non-Gaussian models. These results will be shown in terms of constraints on the σ_8 – f_{NL} plane after marginalizing over the other cosmological and nuisance parameters. The reason for this choice is that, for a fixed Friedmann background, σ_8 and f_{NL} are the two parameters which determine the timing of structure formation and, therefore, the evolution of number density and large-scale clustering of galaxy clusters. In the following, we will always show constraints on the σ_8 – f_{NL} plane at the 68 per cent confidence level.

In analogy with the figure-of-merit introduced to quantify the constraining power of an experiment for the Dark Energy equation of state (e.g., Albrecht et al. 2006, 2009; Wang 2008), we introduce a figure-of-merit for the timing of structure formation in non-Gaussian models:

$$\text{FoM}_{\text{SFT}} = (\det [\text{Cov}(\sigma_8, f_{\text{NL}})])^{-1/2}, \quad (24)$$

where $\text{Cov}(\sigma_8, f_{\text{NL}})$ is the covariance matrix between σ_8 and f_{NL} , which is obtained by inverting the FM and marginalizing over all the other parameters.

In the computation of the FM of Eq.(13), the $N_{l,n}$ number counts are computed out to $z = 2$ within 60 constant redshift bins and within observed mass bins having width $\Delta \log M = 0.1$, extending from the lowest mass limit determined by the selection function (see Fig. 1) and an upper mass limit of $10^{16} h^{-1} M_{\odot}$. We verified that a finer binning does not add more information in the Fisher Matrix. As for the redshift bins, their size is larger than the redshift errors obtainable from optical spectroscopy, and comparable to the typical uncertainties from red-sequence redshift estimates (Gladders et al. 2007).

As for the computation of the FM for the power spectrum of Eq.(18), we used wavenumbers in the range $k_{\text{max}} \geq k \geq 0.001 \text{ Mpc}^{-1}$, independent of redshift. Using an arbitrary small value of k does not change the final results, since extremely large wave modes are not sampled by the surveys and, therefore, do not provide any contribution to the FM. As for the value of k_{max} , the chosen value should represent a compromise between the needs of maximizing the amount of information to be extracted from the survey and of avoiding the contribution of small-scale modes where the validity of the linear bias model is compromised by the onset non-linearity (Percival & White 2009). In the following, we will assume $k_{\text{max}} = 0.3 \text{ Mpc}^{-1}$, and will also show the sensitivity of the results to this choice.

As for the redshift binning, the average cluster power spectrum defined by Eq.(19) is computed by integrating over redshift

³ <http://www.mpe.mpg.de/erosita/MDD-6.pdf>

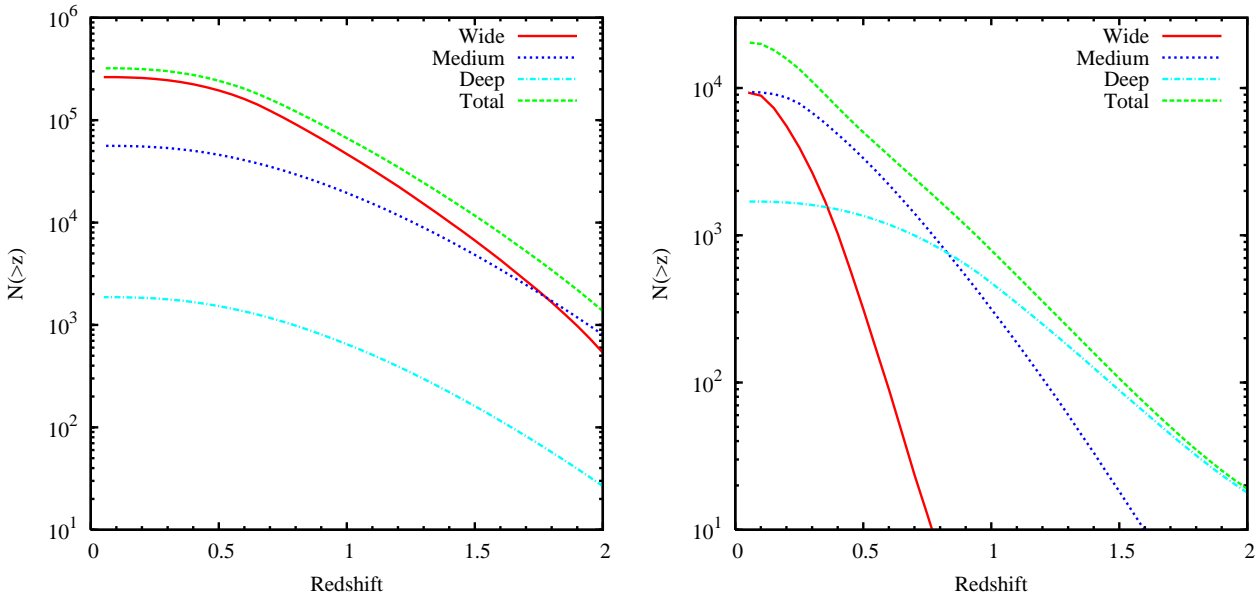


Figure 3. The cumulative redshift distribution for the three surveys. The left panel is for all clusters to be detected down to the survey flux limits, while the right panel is for the clusters in the *bright samples*, corresponding to a 30 times higher flux limit. In both panels solid (red), dotted (blue) and dot-dashed (cyan) curves represent the Wide, Medium and Deep surveys, respectively, while the short-dashed (green) curve represents the sum of the three.

intervals having constant width $\Delta z = 0.2$. This coarser binning, with respect to that used for the analysis of number counts, is dictated by a compromise between the need of extracting the maximum amount of information from the clustering evolution and the request of negligible covariance between adjacent z -intervals (e.g., Stril et al. 2010). Indeed, the contribution from different z -bins can be added in the defining of FM of Eq.(18) only if they carry statistically independent information.

We show in Figure 4 the constraints on the f_{NL} and σ_8 parameters computed from the number counts and from the power spectrum within the Wide survey, by assuming *no prior* on the values of the nuisance parameters. This plot clearly demonstrates the strong complementarity that number counts and large-scale clustering have to constrain σ_8 and f_{NL} : while number counts are highly sensitive to the value of σ_8 , the weak sensitivity of the high-end of the mass function to non-Gaussianity (e.g., Fedeli et al. 2009, and references therein) provides only very weak constraints on f_{NL} ; conversely, the scale-dependence of bias makes the power spectrum a powerful diagnostic for non-Gaussianity, while providing only loose constraints on σ_8 .

If we combine all the information obtainable from the three surveys, we obtain the constraints shown in Figure 5. Most of the constraining power is provided by the Wide survey, with only little information on structure formation timing carried by the Medium and Deep surveys. There are two main reasons for this. First, the Wide survey provides the largest statistical baseline out to $z \simeq 1.5$, when including all clusters down to the mass limit corresponding to detection (see left panel of Figure 3). This implies a better determined mass function and, therefore, stronger constraints on σ_8 . Second, the larger area coverage of the Wide survey allows it to better sample long-wavelength modes, where the scale-dependence of the bias induced by non-Gaussianity can be better assessed, thus turning into stronger constraints on f_{NL} . As shown in Table 2 the value of FOM_{SFT} for the combination of the three surveys is in fact dominated by the Wide Survey.

As already mentioned, we have assumed in our analysis $k_{max} =$

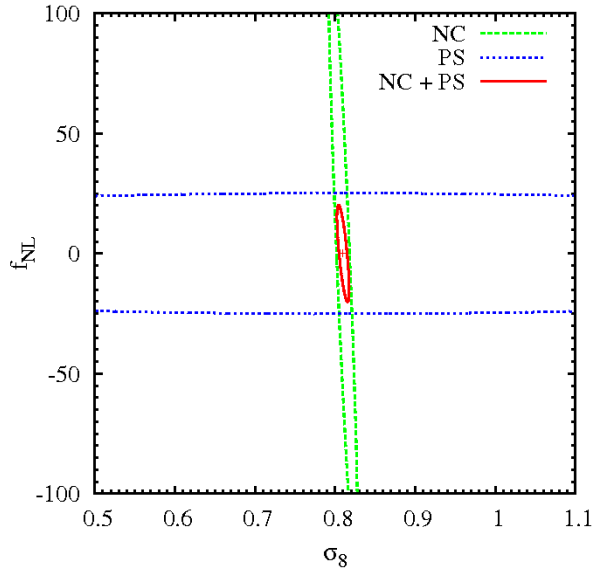


Figure 4. Constraints at the 68 per cent confidence level on non-Gaussian parameter f_{NL} and power spectrum normalization σ_8 coming from number counts alone (short-dashed green curve), power spectrum alone (dotted blue curve) and from the combination of the two (solid red curve). The analysis refer to the clusters detected in the Wide Survey. We marginalized over all the other parameters. *No prior* is assumed for the values of the nuisance parameters. The Fisher Matrix from Planck experiment is included in the calculation of all constraints.

0.3 Mpc^{-1} . In order to quantify the sensitivity of our results to the adopted k_{max} value, we show in Figure 6 how the constraints change for $k_{max} = 0.1 \text{ Mpc}^{-1}$ and $k_{max} = 1 \text{ Mpc}^{-1}$. The smaller value is close to the scale of non-linearity at $z = 0$, although it is probably too conservative at high redshift, $z \sim 1$. As expected, decreasing k_{max} makes the constraints slightly looser, due to the lower

Table 2. Figure-of-merit of structure formation timing, FoM_{SFT} [see Eq. 24], and r.m.s. uncertainty in the non-Gaussian parameter, $\sigma_{f_{\text{NL}}}$, for the three surveys, and for their combination, assuming different priors for the nuisance parameters. Columns 3–6 show the results for the Wide, Medium and Deep Surveys, and for the combination of the three.

		Wide	Medium	Deep	Total
Detection - no pr.	FoM_{SFT}	33.1	8.5	0.4	39.2
	$\sigma_{f_{\text{NL}}}$	11.3	18.5	84.2	10.4
Detection - weak pr.	FoM_{SFT}	33.3	8.8	0.6	39.4
	$\sigma_{f_{\text{NL}}}$	11.3	18.4	84.3	10.4
Detection - strong pr.	FoM_{SFT}	157.2	49.3	3.0	183.2
	$\sigma_{f_{\text{NL}}}$	11.2	18.0	80.9	10.3
Bright - strong pr.	FoM_{SFT}	7.3	14.3	3.0	22.3
	$\sigma_{f_{\text{NL}}}$	55.9	45.9	85.7	33.8

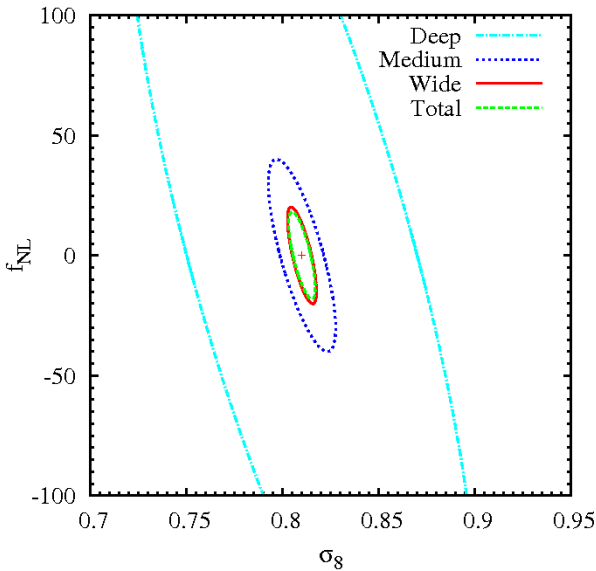


Figure 5. Constraints at the 68 per cent confidence level on non-Gaussian parameter f_{NL} and power spectrum normalization σ_8 from the Deep, Medium and Wide surveys (dot-dashed cyan, dotted blue and solid red curves, respectively), by combining number counts and power spectrum information, by using no priors on the nuisance parameters. Also shown with the short-dashed green curve are the constraints obtained from the combination of the three surveys. *No prior* is assumed for the values of the nuisance parameters. The Fisher Matrix from Planck experiment is included in the calculation of all constraints.

amount of information included in the Fisher Matrix of Eq.(18). Correspondingly, the value of the figure-of-merit decreases from $\text{FoM}_{\text{SFT}} = 39.2$ to 33.1, with the uncertainty on f_{NL} increasing only from $\sigma_{f_{\text{NL}}} = 10.4$ to 12.1. Increasing instead k_{max} to 1 Mpc^{-1} does not lead to any significant improvement of the constraints. In fact, given the level of Poisson noise associated to the cluster distribution, high frequency modes are not adequately sampled and, therefore, adding them to the analysis does not add significant information.

The contribution of information to the Fisher Matrix carried by the power spectrum at different redshifts and wavenumbers can be understood by looking at the dependence of the effective volume, V_{eff} , on the power spectrum, which is set by the bias param-

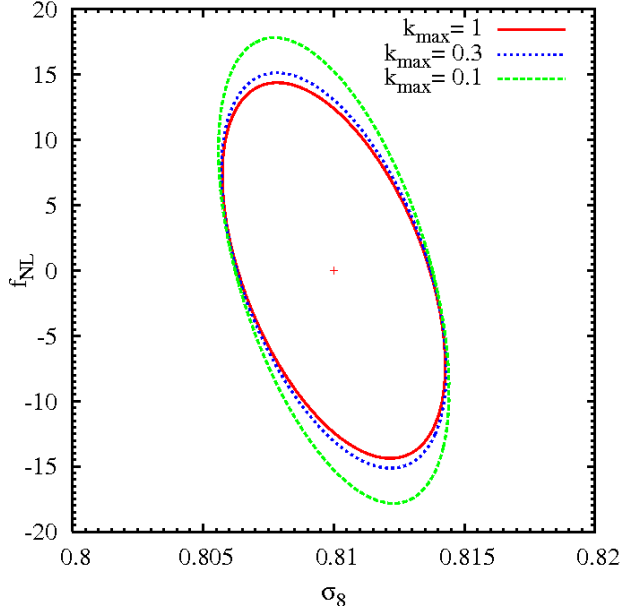


Figure 6. Constraints at the 68 per cent confidence level on non-Gaussian parameter f_{NL} and power spectrum normalization σ_8 from the combination of the three surveys, when changing the maximum value of the wavenumber, k_{max} , for which power spectrum information are included in the Fisher Matrix of Eq.(18). Solid (red), dotted (blue) and short-dashed (green) curves correspond to $k_{\text{max}} = 1, 0.3$ and 0.1 Mpc^{-1} , respectively. *No prior* is assumed for the values of the nuisance parameters. The Fisher Matrix from Planck experiment is included in the calculation of all constraints.

eter, and on the level of Poisson noise, which is set by the number density of clusters. Following Eq.(21), we define the quantity

$$W_v(k, z) = \left[\frac{N(z)\bar{P}_{cl}(k, z)}{1 + N(z)\bar{P}_{cl}(k, z)} \right]^2, \quad (25)$$

which gives the weight carried by the wavenumber k to the computation of the clustering Fisher Matrix at redshift z . In the left panel of Figure 7 we show the redshift dependence of the effective volume computed within redshift intervals of constant width $\Delta z = 0.2$, for different values of k , and compare them to the total comoving volume computed within the same redshift intervals. The effective volume lies always well below the total comoving volume: this is the consequence of the relatively low value of the cluster number density, which makes Poisson noise always dominating. While the total comoving volume V_0 increases with redshift, the effective volume V_{eff} starts declining after reaching a maximum, at $z \approx 0.5$, for all wavenumbers. As for the dependence on k , at a fixed redshift, the value of V_{eff} decreases for both very high and very low values of k . As shown in the right panel of Figure 7, the value of the weight function $W_v(k, z)$ is maximized at $k \approx 0.01 \text{ Mpc}^{-1}$. In fact, for $W_v \ll 1$ (i.e. $N(z)\bar{P}_{cl}(k, z) \ll 1$), the k -dependence of W_v reflects that of \bar{P}_{cl} . Poisson noise is, again, responsible for the low values of W_v , well below unity. Decreasing of the level of this noise would require increasing the number density of objects to be included in the survey. This could be accomplished in principle by decreasing the mass threshold. However, this would require bringing into the surveys low-mass clusters and groups, for which our parametrization of the mass–observable relation may not still be valid.

So far, we presented results by assuming prior on cosmological parameters from Planck experiment and *no prior* knowledge

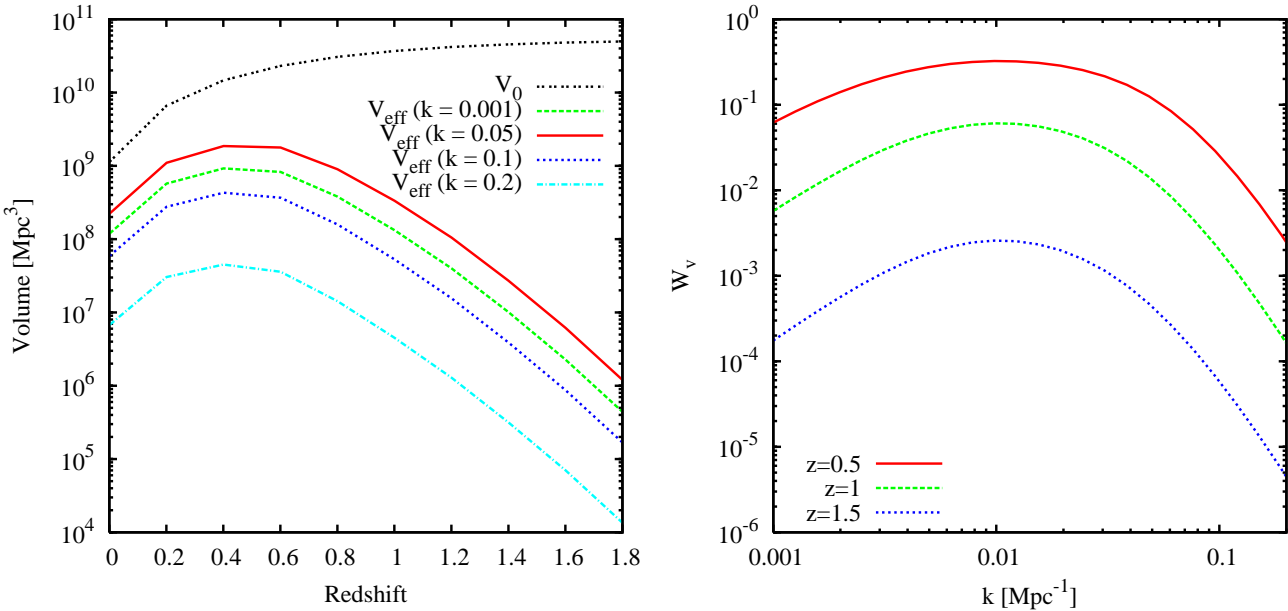


Figure 7. Left panel: the redshift dependence of the effective volume, defined as in Eq.(21), within redshift intervals of constant width $\Delta z = 0.2$, for four values of the wavenumber k . Short-dashed (green), solid (red), dotted (blue) and dot-dashed (cyan) curves correspond to $k = 0.001, 0.05, 0.1$ and 0.2 Mpc^{-1} , respectively. Right panel: the dependence on the wavenumber of the weight $W_v(k, z)$, defined as in Eq.(25), at three different redshifts. Solid (red), dashed (green) and dotted (blue) curves are for $z = 0.5, 1$ and 1.5 , respectively.

on the nuisance parameters. We want to stress that, as already discussed in Sect. 4.2, this is probably too much a conservative approach, in view of the calibration of the relation between robust mass proxies (e.g., Y_X and M_{gas}) and X-ray luminosity for a large number of clusters within the planned surveys. In Figure 8 we show the effect of assuming a prior knowledge of the nuisance parameters. If we assume the *weak priors* for these parameters (see Sect. 4.2), constraints are only slightly improved. Quite interestingly, even assuming the *strong prior* (i.e. nuisance parameters fixed) improves the constraints on σ_8 , while having a smaller impact on those for f_{NL} . Indeed, we find that the error on non-Gaussianity only decrease from $\sigma_{f_{\text{NL}}} \simeq 10.4$ to 10.3 when passing from the *no prior* to the *strong prior* assumption, while the figure-of-merit increases from $\text{FoM}_{\text{SFT}} \simeq 39.2$ to $\simeq 183.2$ (table: 2).

To better understand the reason for the weak dependence of the f_{NL} constraints on the uncertain knowledge of the nuisance parameters, we show in Figure 9 by how much number counts and effective bias change with respect to the value that they take in the Gaussian case, as we vary the mass bias parameter B_M (left panels) and the intrinsic mass-scatter $\sigma_{\ln M}$ (right panels). As a reference value for the non-Gaussianity, we take here $f_{\text{NL}} = 10$, which is comparable to the forecasted precision with which non-Gaussianity can be constrained from our analysis. At $z = 0.5$ the deviation of the number counts from the non-Gaussianity (upper panels) varies only by about one part over thousand when a generous range of variation is allowed for both B_M and $\sigma_{\ln M}$, with only a slightly higher sensitivity to these parameters at $z = 1$. In the bottom panels of Figure 9 we show the sensitivity of the effective bias on nuisance parameters for different values of the wavenumber k . Results are shown at $z = 0.5$ which is close to the redshift where the effective volume V_{eff} reaches its maximum value (see left panel of Figure 7). For the level of non-Gaussianity assumed here, the deviation from the Gaussian effective bias is negligible at the wavenumbers, $k \simeq 0.01 \text{ Mpc}^{-1}$, which are mostly weighted in the computation of the Fisher Matrix (see right panel of Figure 7).

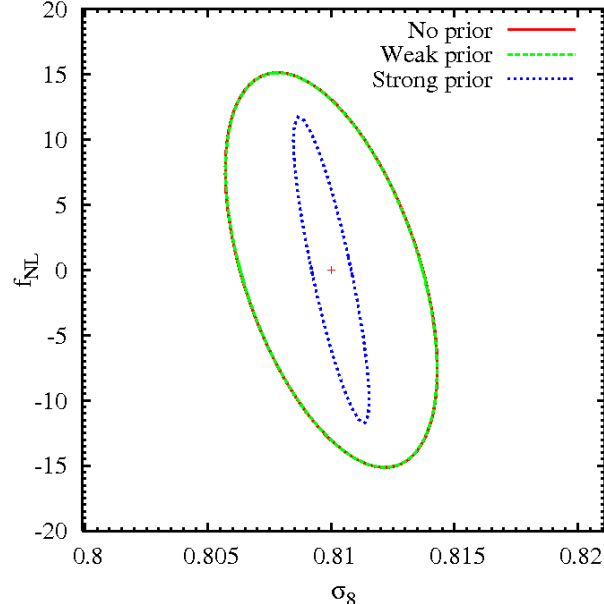


Figure 8. Constraints at the 68 per cent confidence level on the non-Gaussian parameter f_{NL} and power spectrum normalization σ_8 by assuming *no prior* (solid red curve), *weak prior* (dashed green) and *strong prior* (dotted blue) on the nuisance parameters. All constraints are obtained by combining cluster number counts and power spectrum information for the three surveys together. The Fisher Matrix from Planck experiment is included in the calculation of all constraints.

However, as expected, the effect of non-Gaussianity on b_{eff} shows up at very large scales, with a deviation with respect to the Gaussian result by $\gtrsim 40$ per cent for $k \simeq 10^{-3} \text{ Mpc}^{-1}$. This highlights the importance for future surveys to have a highly uniform calibration of the selection function over large area of the sky, for them to be

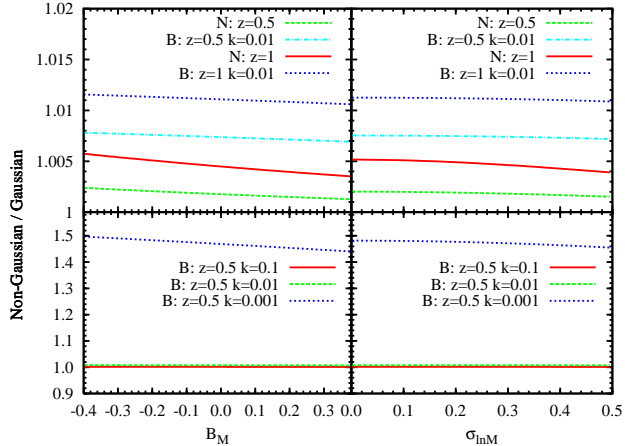


Figure 9. Effect of changing the values of the nuisance parameters of mass bias B_M (left panels) and intrinsic mass scatter $\sigma_{\ln M}$ on the deviations of number counts and effective bias from the Gaussian case. The results shown here are obtained by assuming a mass-limit of $10^{14} M_\odot$. The reference value of non-Gaussianity assumed here is $f_{NL} = 10$. N is the ratio between the redshift distributions in the Gaussian and non-Gaussian cases, while B is the ratio between the effective bias, as defined in equation 20, in the Gaussian and non-Gaussian cases. Upper panels show the results for number counts and effective bias at two different redshifts, $z = 0.5$ and $z = 1$. Lower panels show results for the effective bias at $z = 0.5$ for different wavenumbers, $k = 0.1, 0.01$ and 0.001 Mpc^{-1} .

able to appreciate any subtle scale dependence of the bias parameter. Also in this case, any variation with the value of the nuisance parameters is far smaller than the deviation from Gaussianity. This justifies the weak dependence of the f_{NL} constraints on the uncertain knowledge of the cluster mass calibration.

As already mentioned in Sect. 4.1, the *bright surveys* contain only clusters for which a precise estimate of robust mass proxies, such as Y_X and M_{gas} , can be obtained. In this way, the analysis of the *bright* subsamples offers us the possibility of testing the trade-off between having smaller samples, for which *strong prior* on the nuisance parameters can be assumed, and of larger samples with a less certain knowledge of such parameters. In Figure 10 we show the constraints expected for the *bright* subsamples of the three surveys. We note that this time the role of the Medium and of the Wide surveys are reversed, with the former providing the most stringent constraints. This is not surprising, since the number of bright clusters in the Wide Survey falls below that of the Medium Survey already at $z \approx 0.1$ (see Figure 3). Therefore, the richer statistics of distant clusters in the Medium Survey more than compensates the more efficient sampling of small- k modes offered by the Wide survey. In terms of figure-of-merit, we note that the resulting value from the combination of the three bright surveys is $\text{FoM}_{\text{SFT}} \approx 22.3$: this implies that assuming strong priors for nuisance parameters in the bright surveys has less constraining power than using *no priors* for the surveys defined down to the detection flux limit.

5 DISCUSSION

An interesting outcome of our analysis is the relative lack of sensitivity of the forecasted f_{NL} constraints on the nuisance parameters: constraints on non-Gaussianity are tighter with larger statistics, rather than with a smaller samples with better controlled systematics in cluster mass estimates. While this is the case for the

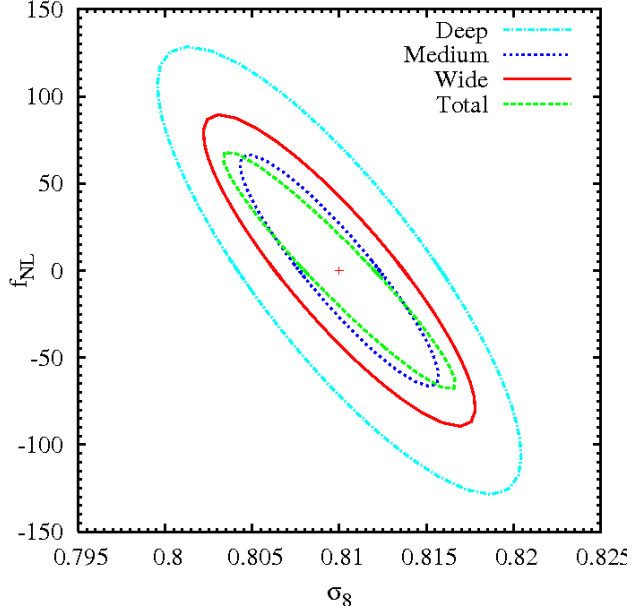


Figure 10. Constraints at the 68 per cent confidence level on the f_{NL} – σ_8 plane for the *bright* subsamples of the three surveys, i.e. by including only clusters with fluxed 30 times larger than the detection flux. Dot-dashed cyan, dotted blue and solid red curves are for the Deep, Medium and Wide surveys, respectively, while the short-dashed green curve is for the combination of the three surveys. We assume here *strong prior* on the nuisance parameters and we include FM from Planck experiment.

purpose of constraining non-Gaussianity, it does not necessarily hold for constraints on the Dark Energy equation of state. In order to quantify the effect of an uncertain knowledge of the nuisance parameters on Dark Energy constraints, we use as a reference the redshift dependence of the equation of state, assumed e.g. in the Dark Energy Task Force (DETF) report (e.g., Albrecht et al. 2009), $w(a) = w_0 + (1 - a)w_a$. Introducing the figure-of-merit $\text{FoM}_{\text{DETF}} = (\det[\text{Cov}(w_0, w_a)])^{-1/2}$, we find $\text{FoM}_{\text{DETF}} \approx 2066$, from the combination of mass function and power spectrum, by adding the contribution of the three surveys and assuming *strong prior* on the values of the nuisance parameters. Such a high value drops to $\text{FoM}_{\text{DETF}} \approx 987$ under the more realistic assumption of *weak priors* on the nuisance parameters, while further reducing only by a small amount, $\text{FoM}_{\text{DETF}} \approx 972$, if we assume no prior on such parameters. Results on the constraining power of the high-sensitivity X-ray surveys reported here on different Dark Energy models will be presented in a future paper.

A first word of caution in the interpretation of such high values of the DETF figure-of-merit lies in the assumption that scatter in the mass bias is always assumed to be log-normal distributed. As discussed by Shaw et al. (2010), deviations from this assumption are in general negligible as long as one relies on mass proxies which have a small value of the scatter, while the uncertain knowledge of the distribution of the scatter may significantly worsen constraints as the scatter increases. In our samples of clusters identified down to the detection limit, cluster selection is based on X-ray luminosity, whose correlation with cluster mass can easily have a scatter as large as 30 per cent. On the other hand, the effect should be much smaller for the *bright* samples, that only contains clusters for which measurements of robust low-scatter mass proxies are available. Restricting our analysis to the *bright surveys*, we find $\text{FoM}_{\text{DETF}} = 423$

and 176 by assuming *strong priors* and *no priors* on the nuisance parameters, respectively.

Another word of caution lies in the assumption that redshifts for all clusters in the surveys are perfectly known. An obvious objection when discussing the cosmological exploitation of large surveys of clusters concerns the possibility of measuring redshifts for all of them. While discussing in detail the synergies between future X-ray and optical/near-IR surveys is beyond the aim of this paper, it is worth pointing out that future imaging and spectroscopic surveys, both ground based (e.g., BigBOSS⁴, PANSTARR⁵, LSST⁶) and from space (e.g., EUCLID⁷, JDEM⁸) will provide either photometric or spectroscopic redshifts for all clusters identified within the WFXT surveys. Furthermore, all clusters in the *bright sample* will have a sufficiently large number of counts to guarantee a rather precise X-ray spectroscopic redshift measurement from the positions of metal lines (Giacconi et al. 2009). In general, uncertainties in redshift measurements could be taken into account in our analysis (e.g., Cunha 2009), at least as long as one has a reliable estimation of redshift errors expected from different observational techniques. While redshifts from optical spectroscopy are generally so accurate that any uncertainty can be neglected, the same is generally not true for photometric redshifts. We also note that no attempt has been pursued so far to assess in detail the reliability of measurements of clusters redshifts from X-ray spectroscopy, as a function of signal-to-noise, cluster temperature and redshift.

In our analysis we did not include the effect of redshift space distortions in the distribution of galaxy clusters induced by peculiar velocities (e.g., Kaiser 1987; White et al. 2009; Desjacques & Sheth 2010). The study of this effect to available galaxy redshift surveys (e.g., Guzzo et al. 2008) has indeed demonstrated that it provides important constraints on the growth rate of density perturbations (see also Linder 2008). Although we expect that its applications to cluster surveys may be limited by the sparser sampling offered by the cluster distribution, the effect of redshift-space distortions should be in principle included when forecasting the cosmological constraining power of future cluster surveys. We will present this analysis in a forthcoming paper.

The analysis presented here demonstrates the potential that future high-sensitivity X-ray cluster surveys could have in constraining possible deviations from Gaussianity. However, it may be worth asking what current data can tell us about such deviations. For instance, a positive skewness has the effect of anticipating the first collapse of massive DM halos. Jee et al. (2009) recently reported the discovery of an unexpectedly massive galaxy cluster at $z \simeq 1.4$, XMMU-J2235.3, identified as part of the initial 11 sq.deg. of the XMM Distant Cluster Project survey (Mullis et al. 2005), having a flux limit of 10×10^{-14} erg s⁻¹ cm⁻². Based on weak lensing (Jee et al. 2009) and X-ray (Rosati et al. 2009) analyses, a robust 1σ lower limit of 5×10^{14} is obtained for the cluster virial mass. By assuming a WMAP-5 cosmology, with $\sigma_8 = 0.81$ and $\Omega_m = 0.28$, and using the mass function by Jenkins et al. (2001), Jee et al. (2009) found that only $\simeq 5 \times 10^{-3}$ of such massive clusters should be expected within the survey area. Thus, they concluded that XMMU-J2235.3 is a rather unlikely event in a standard cosmological scenario. Jimenez & Verde (2009) argued that, for a

fixed value of σ_8 ($= 0.77$ in their analysis) the expected number of such massive clusters can in fact be significantly enhanced in the case of a positively skewed non-Gaussian distribution of primordial perturbations.

In Figure 11 we show the curves in the σ_8 – f_{NL} plane corresponding to different numbers of clusters expected at $z > 1.4$ within 11 sq.deg. and having mass of at least $5 \times 10^{14} M_\odot$. Results are given for the reference non-Gaussian mass function from LoVerde et al. (2008) (dot-dashed curves), that we used for our forecasts, and for the mass function by Matarrese et al. (2000) (solid curves). For both mass functions, we applied the correction to Δ_c suggested by Grossi et al. (2009). As previously discussed, these two mass functions come from different approaches to approximate the exact result for small values of f_{NL} . As expected, the difference between the two mass functions becomes non negligible for $f_{NL} > 100$ for the rare event of such a massive cluster at $z \simeq 1.4$. For each model, the four curves, from right to left, are for 0.05, 0.02, 0.01 and 0.005 such massive clusters found within the survey area, respectively. For homogeneity with the analysis carried out by Jee et al. (2009), we used here the Gaussian mass function by Jenkins et al. (2001). While f_{NL} and σ_8 are left free to vary, all the other cosmological parameters are kept fixed at the fiducial values adopted in our reference cosmological model (see Sect. 3). The results shown in this plot confirm that a positive skewness helps increasing the expected number of clusters. The effect of non-Gaussianity is strongly degenerate with that of changing σ_8 . For instance, increasing the expected number of clusters by about a factor of ten for $\sigma_8 = 0.8$ requires f_{NL} values in excess of the range allowed already at present by CMB (e.g., Komatsu et al. 2010, and references therein) and Large Scale Structure (LSS) (Slosar et al. 2008) data. On the other hand, the same boost in the cluster number can be achieved by requiring $f_{NL} \simeq 100$ and increasing σ_8 to $\simeq 0.87$, again in tension with current CMB and LSS constraints. The conclusion of this analysis is that for XMMU-J2235.3 not to be a very unlikely event, a degree of non-Gaussianity in excess of the currently allowed CMB bounds is required, unless one wants to violate current constraints on σ_8 . Clearly, more than a single detection of such massive distant clusters are needed to draw firm conclusions. However, this example further confirms the strong constraining power of even few massive clusters at $z > 1$. In addition, since galaxy clusters probe much smaller scales than the CMB, they offer a complementary approach to test a possible scale-dependence of non-Gaussianity.

6 CONCLUSIONS

We presented forecasts on the capability of future high-sensitivity X-ray surveys of galaxy clusters to provide constraints on deviations from Gaussian primordial perturbations. Our analysis is based on computing the Fisher Matrix (FM) for the information given by the evolution of mass function and power spectrum of galaxy clusters. Following the approach by Tegmark (1997) to compute the power-spectrum FM (see also Majumdar & Mohr 2004; Rassat et al. 2008; Stril et al. 2010), we include in the analysis the information related to the possible scale-dependence of the linear bias, which represents a unique fingerprint of non-Gaussianity (e.g., Verde 2010, and references therein). According to the self-calibration approach, the model parameters entering in the FM estimate are nine cosmological parameters and 4 nuisance parameters, the latter defining the relation between cluster mass and observable upon which cluster selection is based. Our analysis is based on assuming an observational strategy designed for the Wide Field X-

⁴ <http://bigboss.lbl.gov/>

⁵ <http://pan-starrs.ifa.hawaii.edu/>

⁶ <http://www.lsst.org/>

⁷ <http://arxiv.org/pdf/0912.0914>

⁸ <http://jdem.gsfc.nasa.gov/>

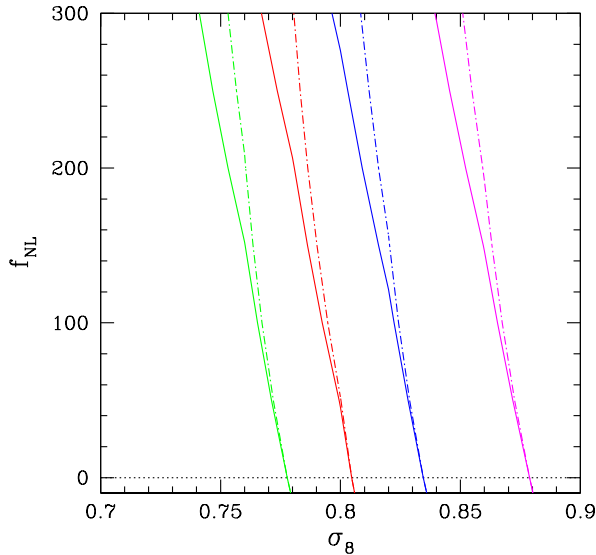


Figure 11. The number of clusters with mass larger than $5 \times 10^{14} M_{\odot}$, found in the redshift range $1.4 < z < 2$ within the same survey area of 11 sq.deg. where the XMMU-J2235.3 cluster has been detected (Jee et al. 2009). Non-Gaussian mass function by LoVerde et al. (2008) (dot-dashed curves) and by Matarrese et al. (2000) (solid curves) are shown. From right to left, magenta, blue, red and green curves show the models on the σ_8 – f_{NL} plane predicting 0.05, 0.02, 0.01 and 0.005 clusters within the survey area, respectively. All other cosmological parameters have been kept fixed to our reference values (see text).

ray Telescope (WFXT, e.g. Giacconi et al. 2009), in which a *Wide* Survey covering most part of the extragalactic sky is complemented by a *Medium* and by a *Deep* Survey (see Table 1). The latter provides mass proxies down to the flux limit for cluster identification in the *Wide* Survey (see Table 1). We showed forecasts for the two parameters that, for a fixed expansion history, define the timing of cosmic structure formation, namely σ_8 and f_{NL} , while marginalizing over all the remaining parameters. Informations on such constraints are quantified by introducing the figure-of-merit for structure formation timing of Eq.(24).

The main results obtained from our analysis can be summarized as follows.

(a) Power spectrum and number counts of galaxy clusters are highly complementary in providing constraints: while the former is sensitive to deviations from Gaussianity, through the scale dependence of the bias, the latter is mostly sensitive to σ_8 .

(b) Most of the constraining power for these two parameters lies in the *Wide* Survey, while the *Medium* and the *Deep* Surveys play an important role for the estimate of X-ray mass proxies for $\simeq 2 \times 10^4$ clusters out to $z \sim 1.5$.

(c) Combining number counts and power spectrum information for the three surveys turns into $\Delta f_{NL} \simeq 10$ for the 1σ uncertainty with which a deviation from Gaussianity associated to a “local shape” model can be constrained. Correspondingly, we find $\text{FoM}_{\text{SFT}} \simeq 39$ for the figure-of-merit of structure formation timing.

(d) Quite interestingly, while the value of FoM_{SFT} significantly worsens when assuming more conservative priors on the nuisance parameters, the above constraint on f_{NL} is weakly sensitive on such priors.

(e) The presence of a cluster as massive as XMMU-J2235.3 at $z \simeq 1.4$ (Jee et al. 2009) turns out to be a rather unlikely event, even allowing for an amount of non-Gaussianity consistent with current CMB (e.g., Komatsu et al. 2010) and LSS (Slosar et al. 2008) constraints. This further demonstrates the strong constraining power of detecting an even small number of massive high- z clusters.

Our analysis lends support to the important role that future cluster surveys will play in constraining deviations from the Gaussian paradigm, with far reaching implications on the primordial mechanisms which seeded density inhomogeneities. The reliability of our forecasts relies on the possibility of calibrating to high precision a universal expression for mass function and large-scale bias. A number of independent groups (Grossi et al. 2007; Dalal et al. 2008; Desjacques et al. 2009; Grossi et al. 2009; Giannantonio & Porciani 2009; Pillepich et al. 2010) carried out large N-body simulations with non-Gaussian initial conditions, finding in general a quite good agreement for the calibration of both mass function and bias. However, the precision required for the calibration of such quantities, for them not to spoil the constraining power of large surveys, is probably higher than what reached at present. First assessments of the impact of uncertainties in the mass function calibration on DE constraints have been already presented (e.g. Wu et al. 2010) and indicate that such uncertainties may not be negligible. There is no doubt that larger suites of non-Gaussian simulations are required to calibrate mass function and large-scale bias also for a range of models beyond the local non-Gaussian models that we considered in the analysis presented here.

A few days after our paper, Cunha et al. (2010) also submitted a paper regarding the study of constraints on non-Gaussian parameter f_{NL} from cluster surveys. They use the Fisher matrix approach applied to the count-in-cell method to extract information on evolution of cluster number density and clustering. Differently from the previous paper by Oguri (2009), Cunha et al. (2010) also included the contribution from covariance between counts in different cells. This allowed them to sample the power spectrum over a large scale range, thus obtaining tighter constraints on f_{NL} than Oguri (2009). By specialising their analysis for the mass selection and sky coverage expected for the DES⁹ optical survey, they forecast a precision of $\sigma_{f_{NL}} \simeq 1\text{--}5$. A detailed comparison between our and their analysis is not straightforward. Besides using different survey specifications, our and their analyses also uses different prescriptions for the mass function and the bias. Just as an example of how sensitive the choice of the bias model is, we verified that excluding the bias correction suggested by Grossi et al. (2009) (the factor $q = 0.75$ that we introduce after Eq.11), the expected errors in f_{NL} would decrease by approximately a factor of 2. This further emphasizes the need for a precise calibration of the model mass function and bias through extended sets of non-Gaussian N-body simulations.

ACKNOWLEDGMENTS.

We acknowledge useful discussions with Cristiano Porciani, Anais Rassat and Paolo Tozzi. We thank Elena Pierpaoli, Ravi Sheth and Licia Verde for useful comments on the first version of this paper. This work has been partially supported by the PRIN-MIUR Grant “The Cosmic Cycle of Baryons”, by a ASI-AAE Theory Grant, by the ASI Contract No. I/016/07/0 COFIS, the ASI/INAF

⁹ <https://www.darkenergysurvey.org/>

Agreement I/072/09/0 for the Planck LFI Activity of Phase E2, the ASI/I/023/05/0 and the ASI/I/088/06/0

REFERENCES

Afshordi N., Tolley A. J., 2008, Phys. Rev. D, 78, 123507

Albrecht A., Amendola L., Bernstein G., Clowe D., Eisenstein D., Guzzo L., Hirata C., Huterer D., et al. 2009, ArXiv e-prints, 0901.0721

Albrecht A., Bernstein G., Cahn R., Freedman W. L., Hewitt J., Hu W., Huth J., Kamionkowski M., et al. 2006, ArXiv e-prints, 0609591

Ameglio S., Borgani S., Pierpaoli E., Dolag K., Ettori S., Morandi A., 2009, MNRAS, 394, 479

Bartolo N., Komatsu E., Matarrese S., Riotto A., 2004, Phys. Rept., 402, 103

Battye R. A., Weller J., 2003, Phys. Rev. D, 68, 083506

Borgani S., Bonometto S. A., 1990, ApJ, 348, 398

Borgani S., Rosati P., Tozzi P., Stanford S. A., Eisenhardt P. R., Lidman C., Holden B., Della Ceca R., Norman C., Squires G., 2001, ApJ, 561, 13

Cappelluti N., Brusa M., Hasinger G., Comastri A., Zamorani G., Finoguenov A., Gilli R., Puccetti S., et al. 2009, A&A, 497, 635

Carbone C., Verde L., Matarrese S., 2008, ApJ, 684, L1

Cash W., 1979, ApJ, 228, 939

Chen X., 2010, ArXiv e-prints, 1002.1416

Colafrancesco S., Lucchin F., Matarrese S., 1989, ApJ, 345, 3

Creminelli P., Senatore L., Zaldarriaga M., Tegmark M., 2007, Journal of Cosmology and Astro-Particle Physics, 3, 5

Crocce M., Fosalba P., Castander F. J., Gaztañaga E., 2010, MNRAS, 403, 1353

Crociani D., Moscardini L., Viel M., Matarrese S., 2009, MNRAS, 394, 133

Cunha C., 2009, Phys. Rev. D, 79, 063009

Cunha C., Huterer D., Dore O., 2010, ArXiv e-prints, 1003.2416

Dalal N., Doré O., Huterer D., Shirokov A., 2008, Phys. Rev. D, 77, 123514

Desjacques V., Seljak U., Iliev I. T., 2009, MNRAS, 396, 85

Desjacques V., Sheth R. K., 2010, Phys. Rev. D, 81, 023526

Eisenstein D. J., Hu W., 1998, ApJ, 496, 605

Ettori S., Morandi A., Tozzi P., Balestra I., Borgani S., Rosati P., Lovisari L., Terenzi F., 2009, A&A, 501, 61

Fedeli C., Moscardini L., Matarrese S., 2009, MNRAS, 397, 1125

Feldman H. A., Kaiser N., Peacock J. A., 1994, ApJ, 426, 23

Gangui A., Lucchin F., Matarrese S., Mollerach S., 1994, ApJ, 430, 447

Giacconi R., Borgani S., Rosati P., Tozzi P., Gilli R., Murray S., Paolillo M., Pareschi G., et al. 2009, in astro2010: The Astronomy and Astrophysics Decadal Survey Vol. 2010 of ArXiv Astrophysics e-prints, Galaxy clusters and the cosmic cycle of baryons across cosmic times. pp 90–+

Giannantonio T., Porciani C., 2009, ArXiv e-prints, 0911.0017

Gladders M. D., Yee H. K. C., Majumdar S., Barrientos L. F., Hoekstra H., Hall P. B., Infante L., 2007, ApJ, 655, 128

Grossi M., Dolag K., Branchini E., Matarrese S., Moscardini L., 2007, MNRAS, 382, 1261

Grossi M., Verde L., Carbone C., Dolag K., Branchini E., Iannuzzi F., Matarrese S., Moscardini L., 2009, MNRAS, 398, 321

Guth A. H., 1981, Phys. Rev. D, 23, 347

Guzzo L., Pierleoni M., Meneux B., Branchini E., Le Fèvre O., Marinoni C., Garilli B., Blaizot J., et al. 2008, Nature, 451, 541

Holder G., Haiman Z., Mohr J. J., 2001, ApJ, 560, L111

Holman R., Tolley A. J., 2008, Journal of Cosmology and Astro-Particle Physics, 5, 1

Hu W., Kravtsov A. V., 2003, ApJ, 584, 702

Jee M. J., Rosati P., Ford H. C., Dawson K. S., Lidman C., Perlmutter S., Demarco R., Strazzullo V., Mullis C., Böhringer H., Fassbender R., 2009, ApJ, 704, 672

Jenkins A., Frenk C. S., White S. D. M., Colberg J. M., Cole S., Evrard A. E., Couchman H. M. P., Yoshida N., 2001, MNRAS, 321, 372

Jimenez R., Verde L., 2009, Phys. Rev. D, 80, 127302

Kaiser N., 1987, MNRAS, 227, 1

Kang X., Norberg P., Silk J., 2007, MNRAS, 376, 343

Komatsu E., Smith K. M., Dunkley J., Bennett C. L., Gold B., Hinshaw G., Jarosik N., Larson D., et al. 2010, ArXiv e-prints, 1001.4538

Komatsu E., Spergel D. N., 2001, Phys. Rev. D, 63, 063002

Kravtsov A. V., Vikhlinin A., Nagai D., 2006, ApJ, 650, 128

Lam T. Y., Sheth R. K., 2009, MNRAS, 395, 1743

Liguori M., Sefusatti E., Fergusson J. R., Shellard E. P. S., 2010, ArXiv e-prints, 1001.4707

Lima M., Hu W., 2004, Phys. Rev. D, 70, 043504

Lima M., Hu W., 2005, Phys. Rev. D, 72, 043006

Linder E. V., 2008, Astroparticle Physics, 29, 336

LoVerde M., Miller A., Shandera S., Verde L., 2008, Journal of Cosmology and Astro-Particle Physics, 4, 14

Maggiore M., Riotto A., 2009, ArXiv e-prints, 0903.1251

Mahdavi A., Hoekstra H., Babul A., Henry J. P., 2008, MNRAS, 384, 1567

Majumdar S., Mohr J. J., 2003, ApJ, 585, 603

Majumdar S., Mohr J. J., 2004, ApJ, 613, 41

Mantz A., Allen S. W., Ebeling H., Rapetti D., Drlica-Wagner A., 2009, ArXiv e-prints, 0909.3099

Mantz A., Allen S. W., Rapetti D., Ebeling H., 2009, ArXiv e-prints, 0909.3098

Matarrese S., Lucchin F., Bonometto S. A., 1986, ApJ, 310, L21

Matarrese S., Verde L., 2008, ApJ, 677, L77

Matarrese S., Verde L., Jimenez R., 2000, ApJ, 541, 10

Mathis H., Diego J. M., Silk J., 2004, MNRAS, 353, 681

Maughan B. J., 2007, ApJ, 668, 772

Meerburg P. D., van der Schaar J. P., Stefano Corasaniti P., 2009, Journal of Cosmology and Astro-Particle Physics, 5, 18

Mo H. J., White S. D. M., 1996, MNRAS, 282, 347

Mullis C. R., Rosati P., Lamer G., Böhringer H., Schwabe A., Schuecker P., Fassbender R., 2005, ApJ, 623, L85

Murray S. S., WFXT Team 2010, in Bulletin of the American Astronomical Society Vol. 41 of Bulletin of the American Astronomical Society, The Wide Field X-ray Telescope Mission. pp 520–+

Nagai D., Vikhlinin A., Kravtsov A. V., 2007, ApJ, 655, 98

Navarro J. F., Frenk C. S., White S. D. M., 1997, ApJ, 490, 493

Oguri M., 2009, Physical Review Letters, 102, 211301

Percival W. J., White M., 2009, MNRAS, 393, 297

Piffaretti R., Valdarnini R., 2008, A&A, 491, 71

Pillepich A., Porciani C., Hahn O., 2010, MNRAS, 402, 191

Pratt G. W., Arnaud M., Piffaretti R., Böhringer H., Ponman T. J., Croston J. H., Voit G. M., Borgani S., Bower R. G., 2010, A&A, 511, A85+

Press W. H., Schechter P., 1974, ApJ, 187, 425

Rapetti D., Allen S. W., Mantz A., Ebeling H., 2009, MNRAS, 400, 699

Rasia E., Mazzotta P., Borgani S., Moscardini L., Dolag K., Tormen G., Diaferio A., Murante G., 2005, *ApJ*, 618, L1

Rassat A., Amara A., Amendola L., Castander F. J., Kitching T., Kunz M., Refregier A., Wang Y., Weller J., 2008, ArXiv e-prints, 0810.0003

Roncarelli M., Moscardini L., Branchini E., Dolag K., Grossi M., Iannuzzi F., Matarrese S., 2010, *MNRAS*, 402, 923

Rosati P., Borgani S., Norman C., 2002, *ARA&A*, 40, 539

Rosati P., della Ceca R., Norman C., Giacconi R., 1998, *ApJ*, 492, L21+

Rosati P., Tozzi P., Gobat R., Santos J. S., Nonino M., Demarco R., Lidman C., Mullis C. R., Strazzullo V., Böhringer H., Fassbender R., Dawson K., Tanaka M., Jee J., Ford H., Lamer G., Schwope A., 2009, *A&A*, 508, 583

Salopek D. S., Bond J. R., 1990, *Phys. Rev. D*, 42, 3936

Schmidt F., Vikhlinin A., Hu W., 2009, *Phys. Rev. D*, 80, 083505

Schuecker P., Böhringer H., Collins C. A., Guzzo L., 2003, *A&A*, 398, 867

Sefusatti E., Vale C., Kadota K., Frieman J., 2007, *ApJ*, 658, 669

Shang C., Haiman Z., Verde L., 2009, *MNRAS*, 400, 1085

Shaw L. D., Holder G. P., Dudley J., 2010, *ApJ*, 716, 281

Sheth R. K., Mo H. J., Tormen G., 2001, *MNRAS*, 323, 1

Sheth R. K., Tormen G., 1999, *MNRAS*, 308, 119

Sheth R. K., Tormen G., 2002, *MNRAS*, 329, 61

Slosar A., Hirata C., Seljak U., Ho S., Padmanabhan N., 2008, *Journal of Cosmology and Astro-Particle Physics*, 8, 31

Stril A., Cahn R. N., Linder E. V., 2010, *MNRAS*, 404, 239

Taruya A., Koyama K., Matsubara T., 2008, *Phys. Rev. D*, 78, 123534

Tegmark M., 1997, *Physical Review Letters*, 79, 3806

Tinker J., Kravtsov A. V., Klypin A., Abazajian K., Warren M., Yepes G., Gottlöber S., Holz D. E., 2008, *ApJ*, 688, 709

Valageas P., 2010, *A&A*, 514, A46+

Verde L., 2010, ArXiv e-prints, 1001.5217

Verde L., Matarrese S., 2009, *ApJ*, 706, L91

Verde L., Wang L., Heavens A. F., Kamionkowski M., 2000, *MNRAS*, 313, 141

Vikhlinin A., Burenin R. A., Ebeling H., Forman W. R., Hornstrup A., Jones C., Kravtsov A. V., Murray S. S., et al., 2009, *ApJ*, 692, 1033

Vikhlinin A., Kravtsov A. V., Burenin R. A., Ebeling H., Forman W. R., Hornstrup A., Jones C., Murray S. S., et al., 2009, *ApJ*, 692, 1060

Vikhlinin A., Murray S., Gilli R., Tozzi P., Paolillo M., Brandt N., Tagliaferri G., Bautz M., et al., 2009, in *astro2010: The Astronomy and Astrophysics Decadal Survey Vol. 2010* of ArXiv Astrophysics e-prints, X-ray Cluster Cosmology. pp 305–+

Voges W., Aschenbach B., Boller T., Bräuninger H., Briel U., Burkert W., Dennerl K., Englhauser J., et al., 1999, *A&A*, 349, 389

Voit G. M., 2005, *Reviews of Modern Physics*, 77, 207

Wang Y., 2008, *Phys. Rev. D*, 77, 123525

Warren M. S., Abazajian K., Holz D. E., Teodoro L., 2006, *ApJ*, 646, 881

White M., Song Y., Percival W. J., 2009, *MNRAS*, 397, 1348

Wu H., Zentner A. R., Wechsler R. H., 2010, *ApJ*, 713, 856

Yadav A. P. S., Komatsu E., Wandelt B. D., 2007, *ApJ*, 664, 680

Yadav A. P. S., Wandelt B. D., 2008, *Physical Review Letters*, 100, 181301

Zhang Y., Okabe N., Finoguenov A., Smith G. P., Piffaretti R., Valdarnini R., Babul A., Evrard A. E., et al., 2010, *ApJ*, 711, 1033